

Electronic Thesis and Dissertation Repository

---

2-8-2022 9:30 AM

## Material Characterization of Compression Molded Composites

Broderic Clement-Thorne, *The University of Western Ontario*

Supervisor: Hrymak, A., *The University of Western Ontario*

Co-Supervisor: Henning, F., *Fraunhofer Institute for Chemical Technology*

A thesis submitted in partial fulfillment of the requirements for the Master of Engineering Science degree in Mechanical and Materials Engineering

© Broderic Clement-Thorne 2022

Follow this and additional works at: <https://ir.lib.uwo.ca/etd>



Part of the [Materials Science and Engineering Commons](#)

---

### Recommended Citation

Clement-Thorne, Broderic, "Material Characterization of Compression Molded Composites" (2022).  
*Electronic Thesis and Dissertation Repository*. 8423.  
<https://ir.lib.uwo.ca/etd/8423>

This Dissertation/Thesis is brought to you for free and open access by Scholarship@Western. It has been accepted for inclusion in Electronic Thesis and Dissertation Repository by an authorized administrator of Scholarship@Western. For more information, please contact [wlsadmin@uwo.ca](mailto:wlsadmin@uwo.ca).

## Abstract

Composite materials are widely used in the automotive industry to keep cost and weight down. The ability to simulate the fabrication of parts is an important way to use resources effectively. The molding process can also have very dramatic effects on material properties. These properties are determined by the microstructure of the polymer composite material, including the length, concentration, and orientation of the fibers used as reinforcement. Therefore this study seeks to characterize the material properties of a long glass fiber reinforced polyamide composite, the effects of molding conditions on those material properties, and characterization of the microstructure of the polymer composite under different processing conditions. It was found that material flow affects fiber orientation, including simple geometry changes, and that this material had an inherent fiber alignment from the initial state. Fiber length and concentration throughout the polymer composite part was found to be very consistent under all processing conditions investigated.

## Keywords

Composite, materials engineering, polyamide, glass matt thermoplastic, compression molding, microcomputed tomography, microstructure, characterization

## Summary for Lay Audience

Composite materials have become a staple for the automotive industry. One method of composite fabrication that is very effective for light and strong semi-structural parts is compression molding, where a material is formed into a shape using heat and pressure. For effective use of time, money, and materials, being able to simulate compression molding is greatly desired. A successful simulation needs a variety of input parameters relating to the material properties. Some of the key properties include the fiber volume concentration, fiber length, and fiber orientation, which are part of the materials microstructure. In addition, there is interest in understanding how the various molding conditions will affect those properties due to material flow, mold and material temperatures, and part geometry.

This study aims to characterize the microstructure of two simple parts: a plaque and a hat section. Both parts have been compression molded using Lanxess Tepex Flowcore, a glass-fiber/polyamide-6 composite. The reason that simple parts are being characterized is to provide a baseline for simulation validation, and to be able to isolate differences in molding conditions such as having the material undergo significant flow, but with no geometry changes.

The results show that fiber length remains very consistent regardless of molding conditions, and that part geometry influences the microstructure, specifically the fiber orientation. It was also found that the initial unmolded material has an inherent fiber alignment.

## Acknowledgments

I would like to thank my supervisor throughout this project, Professor Andrew Hrymak, for his patience, guidance, incredibly helpful advice, and kind mentorship. I would also like to thank Professor Frank Henning, for his advice and support.

I would like to thank Professor Anthony Straatman, a member of my advisory committee, for his advice and his time.

I would like to thank Stanislav Ivanov, Navraj Heer, and the rest of the Fraunhofer Project Center team for their advice and help with running experiments, molding my parts, and providing an excellent study space to use while my tests were running.

I would like to thank Ryan Gergely from General Motors for the advice, resources, and support he gave throughout this project.

I would like to thank Trevor Sabiston from Waterloo for running the fiber orientation analysis, and Dominik Dörr for all the advice and help he gave.

I would like to thank my groupmates, especially Thomas Chang and Cheng Xu, who helped me work through many problems and always made me feel at ease.

I would like to thank the staff at Surface Science Western, especially Ivan Barker, for the training and use of the microscopy and microcomputed tomography equipment.

I would also like to thank my girlfriend Megan, for her continued support of me pursuing this degree, and without who I would have never finished.

# Table of Contents

Abstract.....	ii
Summary for Lay Audience.....	iv
Acknowledgments.....	v
Table of Contents.....	vi
List of Tables.....	ix
List of Figures.....	x
List of Appendices.....	xiii
Chapter 1.....	1
1 Introduction.....	1
1.1 Scope.....	1
1.2 Motivation.....	1
1.3 Structure of Thesis.....	2
Chapter 2.....	3
2 Review.....	3
2.1 Glass Mat Thermoplastics and Compression Molding.....	3
2.2 Mechanical Testing.....	4
2.2.1 Maximum Tensile Stress, $\sigma$ .....	4
2.2.2 Maximum Tensile Strain, $\epsilon$ .....	5
2.2.3 Young's Modulus of Elasticity, $E$ .....	6
2.2.4 Flexural Modulus of Elasticity, $E_{\text{bend}}$ .....	7
2.3 Fiber Concentration.....	8
2.4 Fiber Length.....	9
2.5 Fiber Orientation.....	10
2.5.1 Method of Ellipses.....	12

2.5.2	Micro-Computed Tomography .....	13
Chapter 3	.....	15
3	Experimental Characterization.....	15
3.1	Flowcore Specifications.....	15
3.2	Manufacturing of Molded Parts .....	17
3.2.1	Part Types .....	17
3.2.2	Molding Conditions .....	17
3.2.3	Sample Preparation .....	18
3.3	Fiber Length Measurements .....	19
3.4	X-Ray Micro-Computed Tomography .....	20
3.5	Microscopy .....	23
Chapter 4	.....	25
4	Results.....	25
4.1	Mechanical Properties.....	25
4.1.1	Plaque.....	25
4.1.2	Hat Section.....	29
4.2	Fiber Concentration.....	31
4.2.1	Fiber Concentration in Source Material.....	31
4.2.2	Effect of Flow on Fiber Concentration .....	32
4.2.3	Effect of Part Geometry on Fiber Concentration.....	35
4.3	Fiber Length.....	36
4.4	Fiber Orientation .....	38
4.4.1	Optical Microscopy.....	39
4.4.2	Micro-Computed Tomography Validation .....	42
4.4.3	Micro-Computed Tomography .....	45
Chapter 5	.....	52

5 Conclusion and Future Work .....	52
References.....	54
Appendices.....	56
Curriculum Vitae .....	64



## List of Tables

Table 3-1 Flowcore Material Manufacturer Information.....	15
Table 3-2 Manufacturer Provided Mechanical Properties of Flowcore.....	16
Table 3-3 Manufacturer Provided Thermal Properties of Flowcore.....	16
Table 3-4 Molding Conditions of Plaque and Hat Section.....	18
Table 4-1 Fiber Weight Percent of Plaques and Unmolded Samples.....	34
Table 4-2 Hat Section Fiber Weight Percent by Location.....	36
Table 4-3 Results of Fiber Length Measurements.....	38
Table 4-4 Fiber Orientation Sample Naming Convention.....	39
Table 4-5 Averages of Microscopy Samples Components of Fiber Orientation.....	40
Table 4-6 Fiber Orientation Tensor Component Changes with Flow in 62.4% Charge Coverage.....	48
Table 4-7 Comparison of Average Values of Primary Components of Orientation $a_{11}$ and $a_{22}$ of Hat Section.....	51

# List of Figures

Figure 2-1 Process steps of GMT Compression Molding .....	4
Figure 2-2 Sample Shape Used in Tensile Tests, as per ASTM D638 .....	5
Figure 2-3 Tensile Test Sample Dimensions .....	6
Figure 2-4 Stress-Strain Curve for 0° Orientation Plaque Tensile Sample .....	7
Figure 2-5 Three-Point-Bending Test Diagram .....	8
Figure 2-6 Kelly-Tyson Prediction of Fiber Length vs Tensile Strength Graph (J. L. Thomason, 29) .....	10
Figure 2-7 Example of Imaged Material Split into Eight Bins .....	11
Figure 2-8 Fiber Orientation Coordinate Convention .....	12
Figure 2-9 Method of Ellipses Diagram, In-Plane Angle ( $\theta_f$ ), Out-Of-Plane Angle ( $\theta_f$ ) [Velez-Garcia, 13] .....	13
Figure 2-10 Simplified micro-computed tomography sampling .....	14
Figure 3-1 Hat Section Diagram, Top Down (Left), Profile (Right) .....	17
Figure 3-2 Example of Matrix Burn Off, Before (Left) and After (Right) .....	19
Figure 3-3 Imaged Fibers for Length Measurement (Cropped) .....	20
Figure 3-4 Using ImageJ 'Measure' Tool to Follow the Fiber Curve .....	20
Figure 3-5 Standard uCT Sample (Left) vs Stacked Disc Samples (Right) .....	21
Figure 3-6 Slice of uCT Scan of 10 Samples .....	22
Figure 3-7 uCT Scan of Individual Sample Pre-Alignment .....	22
Figure 3-8 uCT Scan of Individual Sample Post-Alignment .....	23

Figure 4-1 Effect of Heating Time on Young's Modulus in 100% Coverage Molded Plaques .....	26
Figure 4-2 Mechanical Test Sampling Locations in 100% Coverage Plaques.....	27
Figure 4-3 Effect of Orientation on Young's Modulus of ST Coupons from 100% Coverage Molded Plaques.....	27
Figure 4-4 Effect of Material Flow on Young's Modulus .....	28
Figure 4-5 Sampling Locations of 90° Samples for Plaques with 90% (Left) and 62.4% (Right) Charge Coverage .....	28
Figure 4-6 Hat Section Labeling Diagram.....	29
Figure 4-7 Comparison of Flexural Modulus in Hat Section Sample Areas at 90° Orientation to Machine Direction .....	30
Figure 4-8 Comparison of Flexural Modulus Between All Locations of Plaques and Hat Sections.....	31
Figure 4-9 Plaque Concentration Sampling Diagram for 90% Charge Coverage (Left) and 62.4% Charge Coverage (Right).....	32
Figure 4-10 Fiber Weight Percent Throughout Plaques with 90% (Left) and 62.4% (Right) Charge Coverages .....	33
Figure 4-11 Hat Section Fiber Weight Percent Graph.....	35
Figure 4-12 Hat Section Fiber Weight Percent by Location.....	36
Figure 4-13 Fiber Length Test Sample Location: Plaque.....	37
Figure 4-14 Fiber Length Test Sample Location: Hat Section.....	37
Figure 4-15 Fiber Length Distribution Graph of Unmolded Sheets, Plaques, and Hat Sections .....	38

Figure 4-16 Optical Microscopy $a_{11}$ Orientation Compilation .....	40
Figure 4-17 Optical Microscopy $a_{22}$ Orientation Compilation .....	41
Figure 4-18 Optical Microscopy $a_{33}$ Orientation Compilation .....	41
Figure 4-19 Averaged Orientation Components of All 8 Microscopy Samples.....	42
Figure 4-20 uCT and OM Comparison of $a_{11}$ .....	43
Figure 4-21 uCT and OM Comparison of $a_{22}$ .....	44
Figure 4-22 uCT and OM Comparison of $a_{33}$ .....	45
Figure 4-23 uCT Plaque Sample Locations for Different Initial Charge Coverage .....	46
Figure 4-24 $a_{11}$ across Locations C, F, and B of 62.4% Coverage Plaques.....	47
Figure 4-25 $a_{22}$ across Locations C, F, and B of 62.4% Coverage Plaques.....	47
Figure 4-26 $a_{33}$ across Locations C, F, and B of 62.4% Coverage Plaques.....	48
Figure 4-27 Increase of $a_{22}$ and Decrease of $a_{11}$ in Hat Section Parts as Material Travels Through Z-Axis .....	50

## List of Appendices

Appendix A - Comparison of Average Values of Primary Components of Orientation $a_{11}$ and $a_{22}$ of Hat Section Secondary Locations .....	56
Appendix B - Orientation Sampling Locations and Molding Conditions of Plaques.....	56
Appendix C - Orientation Sampling Locations and Molding Conditions of Hat Sections.....	59
Appendix D - Orientation Sampling Location Figures and Associated Sample Numbers.....	61

# Chapter 1

## 1 Introduction

### 1.1 Scope

The aim of this master's thesis is to study the effects of processing of a novel glass-mat thermoplastic composite (GMT), specifically targeting the post-molding microstructure characterization. The material being examined is Lanxess Tepex Flowcore, a glass fiber reinforced polyamide-6 matrix composite, in two different compression molded parts: a plaque and a hat section.

The effect of molding conditions and part geometry on mechanical properties such as tensile strength and Young's modulus, as well as their effect on the microstructure components of fiber orientation, length, and concentration are examined. While some of the material properties have been provided by the material manufacturer, further investigation of the microstructure is undertaken to provide sufficient information for computer simulation validation studies.

### 1.2 Motivation

High-performance low-density materials are a requirement for the modern automotive industry. In addition to reducing automobile operating cost for the consumer, as components are lighter thus making the vehicles more fuel efficient, reducing greenhouse gas emissions for internal combustion vehicles and extending the range of electric drive vehicles [26]. Fiber reinforced polymer composites are at the forefront of lightweighting component technologies due the weight-to-strength properties. Compression molded GMTs offer a compelling option for the automotive industry, which allows for complicated geometries of semi-structural parts with attractive cost, weight, and strength ratios [27].

The ability to simulate and predict composite part production and performance is necessary for the automotive industry to adopt polymer composites on a widespread scale. This research provides microstructure characterization of molded parts, including

the effects of part geometry and mechanical properties. The microstructure characterization is necessary for computer simulation of the process to be conducted, both as a starting point and for validation. This work is done in parallel with the work of Thomas Chang, who is examining the same material, but in parts with significantly more complicated geometry [27].

### 1.3 Structure of Thesis

This thesis is divided into five (5) chapters. The first chapter covers the motivation for this thesis, introduction, and thesis overview. Chapter 2 covers a review of the relevant literature and background information, such as desired material properties, testing standards required and related previous research. Chapter 3 explores the experimental characterization of the material, including the methods for sample preparation and a breakdown of how non-standardized tests for fiber length and orientation were developed and run. Chapter 4 discusses the results obtained, and Chapter 5 is a conclusion with comments on future work.

## Chapter 2

### 2 Review

#### 2.1 Glass Mat Thermoplastics and Compression Molding

Glass mat thermoplastics (GMTs) are made of a glass mat with either continuous or discontinuous fibers and a thermoplastic. Continuous fibers in this setting describes fibers that are not cut prior to being incorporated to the GMT and run the entire length of the part. Discontinuous fibers are chopped at a specific length before being added to the GMT. The glass mat serves as the reinforcement, while the thermoplastic is the matrix, creating a composite material [1]. The specific GMT composite studied here is a commercial product Lanxess Tepex Flowcore. The thermoplastic being used is polyamide 6 (PA6), with the fibers being E-glass rovings. GMTs are produced by laminating continuous-discontinuous glass fibers with the thermoplastic between large rollers at a high temperature, then cooling the continuous sheet and chopping it into usable blanks [2]. Flowcore is a chopped GMT, meaning the glass fibers have been cut to a specific length before laminating (in this case, 50mm). Chopped GMTs have better flow during the compression molding process compared to continuous fiber GMTs, and the shorter fibers allow for more complex geometry in the molded parts. The cut blanks of GMTs normally range from 1m-1.5m by 1m-1.5m, with a thickness of 1mm-5mm [1].

Before being molded, the blanks must be heated. An infrared oven is commonly used to perform the heating and can quite often have a conveyer belt running through it, allowing for the smooth addition of new blanks to the oven [2]. After heating, the blank is placed inside a mold, and compressed at a pressure ranging from 5MPa to 30MPa. A heated mold is used to increase flowability, ranging from 20°C to 150°C depending on the thermoplastic. A mold will typically be held closed and under pressure for around 60 seconds [3]. Figure 2-1 illustrates a schematic of the molding process.



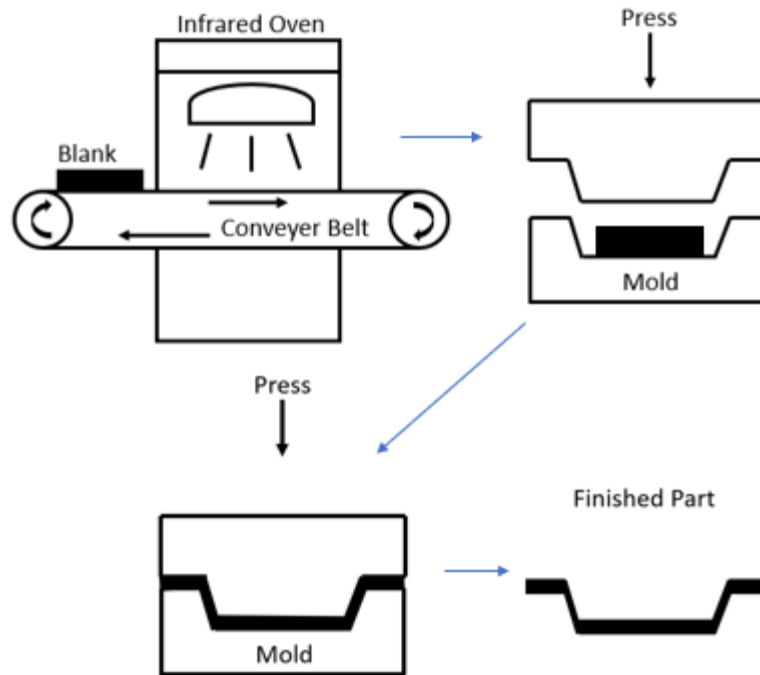


**Figure 2-1 Process steps of GMT Compression Molding**

## 2.2 Mechanical Testing

The properties that are being measured are maximum tensile stress, maximum tensile strain, Young's modulus of elasticity, and the flexural modulus of elasticity. Two types of tests were run to find these properties, a tensile test and a three-point bending test, following ASTM standards D638 [23] and D7264 [24], respectively.

### 2.2.1 Maximum Tensile Stress, $\sigma$

Tensile or normal stress is defined as force over area. The maximum tensile stress, also referred to as engineering stress, is the maximum force,  $F$ , over the original cross-sectional area,  $A_0$ , before breaking. A higher maximum tensile stress means the material can withstand a greater force before breaking [4].

$$\sigma = \frac{F}{A_0} \quad (2.2.1)$$

### 2.2.2 Maximum Tensile Strain, $\epsilon$

Tensile or normal strain is defined as the change of a materials length ( $\delta$ ) over its original length ( $L_0$ ) when subjected to a force ( $P$ ), shown in Figure 2-2. The maximum tensile strain is the maximum length change relative to its original length a material can take before breaking. A higher maximum tensile strain means a material can withstand a larger change in length before breaking [4]. Figure 2-3 shows the dimensions of the test samples used in this study. A video extensometer was used to measure the change in length, where the gauge length of the samples was freckled with dots of paint and a video camera tracked the distance between two dots as the sample underwent stress.

$$\epsilon = \frac{L - L_0}{L_0} \quad (2.2.2)$$

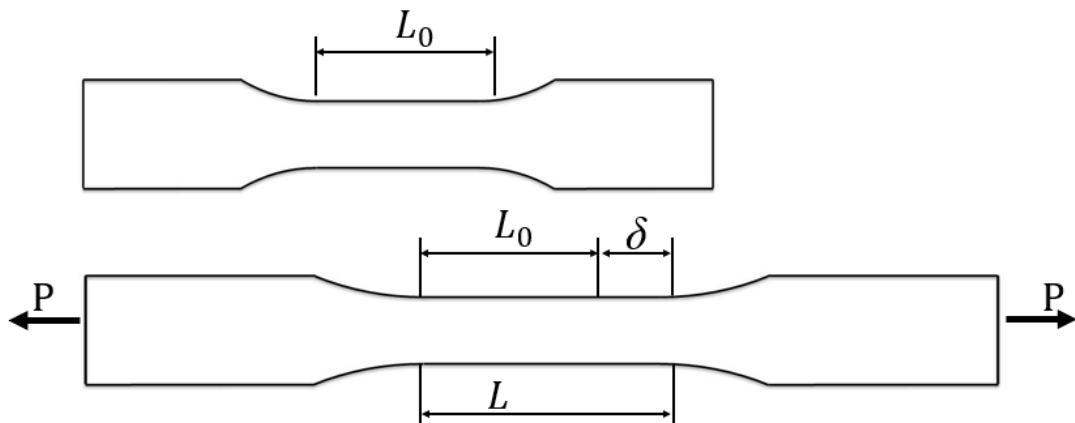


**Figure 2-2 Sample Shape Used in Tensile Tests, as per ASTM D638**

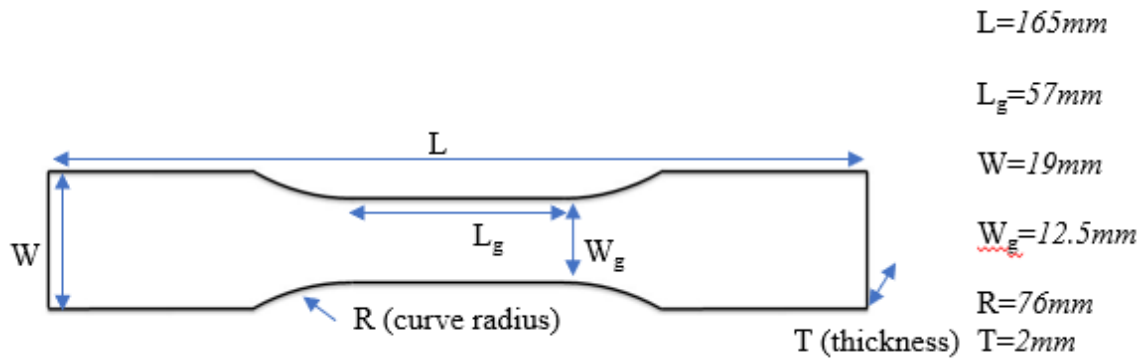


**Figure 2-3 Tensile Test Sample Dimensions**

### 2.2.3 Young's Modulus of Elasticity, E

The modulus of elasticity, or Young's modulus, represents the slope of a stress-strain curve within the elastic region, the region of material behaviour where the sample after deformation will return to its original dimensions. A higher Young's modulus means that a material needs to have more stress applied to it to make the same strain occur, or more simply, a higher force to create the same change in length [4]. For this study, Young's Modulus was calculated from strain values 0.001 to 0.003, as shown in Figure 2-4. This was done in the initial linear portion of the stress-strain curve, as it can be difficult to estimate Young's Modulus in a material where the stress-strain curve has curvature.

$$E = \frac{\text{Stress}}{\text{Strain}} = \frac{\sigma}{\epsilon} \quad (2.2.3)$$

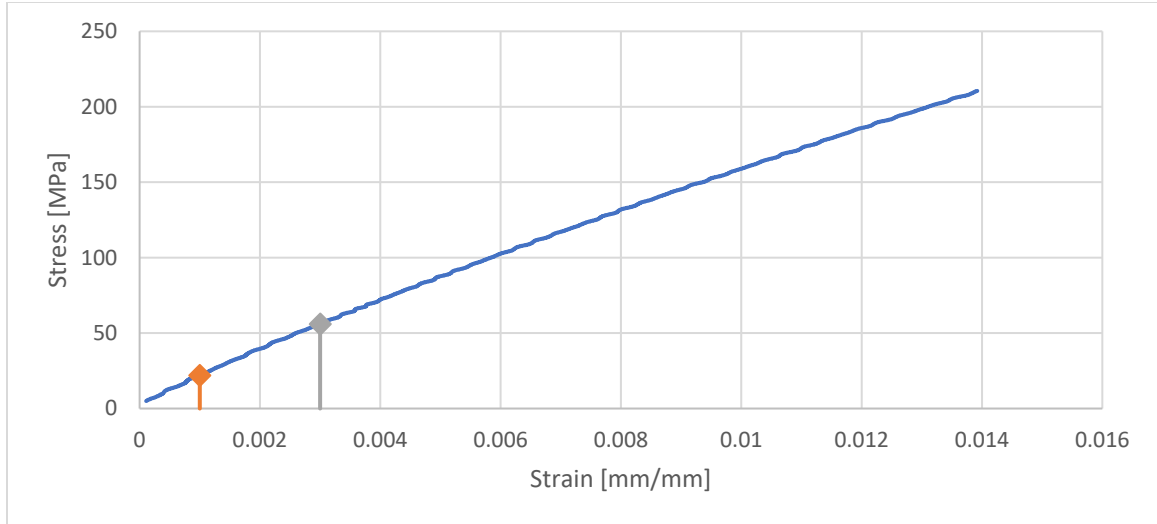


**Figure 2-4 Stress-Strain Curve for 0° Orientation Plaque Tensile Sample**

#### 2.2.4 Flexural Modulus of Elasticity, $E_{bend}$

The flexural modulus of elasticity is defined in much the same way as Young's modulus of elasticity, as the ratio between stress and strain, however it is found in a different way. Young's modulus is found through tension and compression of a material, while the flexural modulus is found through the bending of a material [4].

$$E_{bend} = \frac{L^3 F}{4wh^3 d} \quad (2.2.4)$$

Illustrated in Figure 2-5,  $L$  is the length of a beam,  $w$  is the width of a beam,  $h$  is the height of a beam,  $F$  is the force applied to the center of the beam, and  $d$  is the deflection of the beam.

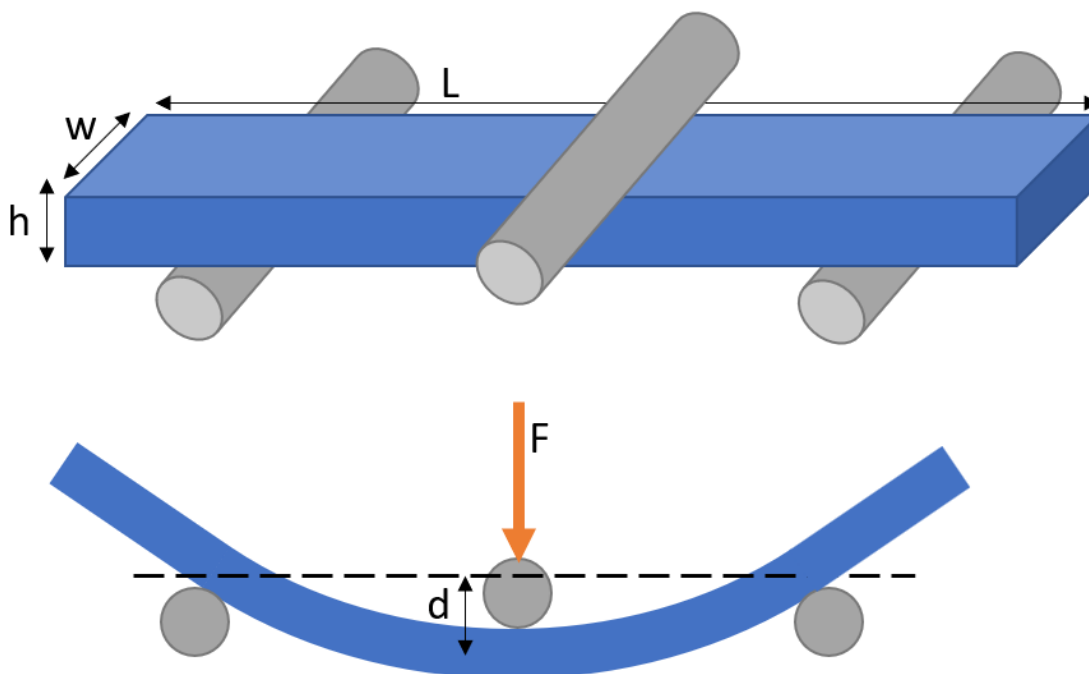


**Figure 2-5 Three-Point-Bending Test Diagram**

### 2.3 Fiber Concentration

The concentration of fibers present in the composite material is important to validate computer simulations, as well as for calculating the theoretical limits of mechanical properties [5]. By weighing the sample before ( $M_i$ ) and after ( $M_f$ ) burning off the matrix, either in a furnace or in a thermogravimetric analyzer (TGA), the weight percent ( $Wt\%$ ) of the fibers can be found, as shown in Equation 2.3.1.

$$Wt\% = \frac{M_f}{M_i} \quad (2.3.1)$$

A TGA is ideal for this, as it allows for the process to be done in an environment without oxygen. The chamber with the samples is flooded with nitrogen and raised past the thermal decomposition temperature of the matrix, meaning the matrix does not actually burn, but breaks down into a gas, leaving only the fibers behind. ASTM D3171, Procedure G, [25] is the testing standard used to determine the fiber concentration.

The fiber volume percent (*Vol%*) is also useful [10] and can be derived from the weight percent, provided the densities of the composite ( $\rho_c$ ) and reinforcement ( $\rho_r$ ) are known. This calculation is shown in Equation 2.3.2.

$$Vol\% = \frac{M_f}{M_i} \times \frac{\rho_c}{\rho_f} \times 100 \quad (2.3.2)$$

## 2.4 Fiber Length

Generally, increased fiber reinforcement length is correlated with increased mechanical properties of the composite. Fibers can be considered “short” if they are 1mm or less in length, and “long” if they are greater than 1mm in length [30]. Figure 2-6 provides the trends of tensile strength versus fiber length for a glass fiber-reinforced polypropylene composite. The fiber aspect ratio ( $s$ ), the ratio between fiber length ( $L$ ) and fiber diameter ( $d$ ) is an important factor in determining the effect of fiber length on material properties. Bartos et al [6] have done extensive testing into the effects of the fiber length, diameter, and aspect ratio on the mechanical properties of polymer composites. The fiber aspect ratio is used to determine theoretical strengths and limits of a composite material, such as the interfacial shear stress and stress transfer length [1]. Fibers can break during the molding process due to the local shear from pressure and flow geometry changes, which could then greatly influence the local part properties.

$$s = \frac{L}{d} \quad (2.4)$$

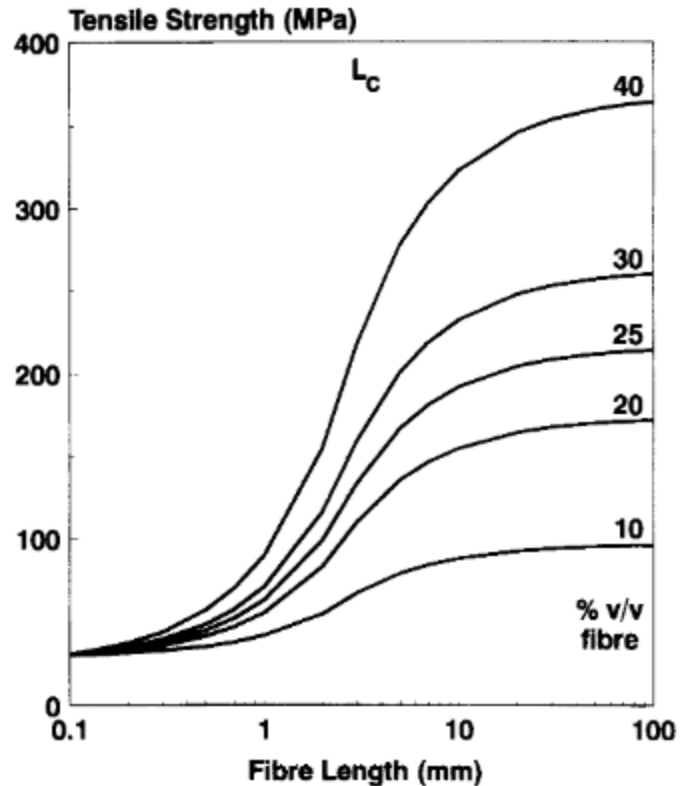


**Figure 2-6 Kelly-Tyson Prediction of Fiber Length vs Tensile Strength Graph (J. L. Thomason, 29)**

The material being examined in this study has fibers primarily in a planar distribution due to the geometry of the parts, the fibers being significantly longer than the part thickness, and the nature of GMT construction [7]. Fiber length distribution can easily be found from molded parts by burning off the matrix and sampling the remaining fibers. Dahl et al [8] developed a robust technique for fiber length measurements. A breakdown of the sampling and measuring technique that was developed based on their approach can be found in section 3.2, *Fiber Length Measurements*.

## 2.5 Fiber Orientation

As fiber orientation is critically important in the analysis and prediction of composite material properties [9], it is equally important to have a robust way of finding and displaying the orientation information. Fiber orientation data of a composite is displayed with a fiber orientation tensor (FOT), which is the probability function of any individual

fiber being aligned with a cardinal direction at that point in the composite. The classic tensor form can be seen in Equation 2.5. The tensor is broken down into three principal components,  $a_{11}$ ,  $a_{22}$ , and  $a_{33}$ , which are in bold in Equation 2.5. The probability of  $a_{11}$ ,  $a_{22}$ , and  $a_{33}$  at any given point always add up to 1.0. If a fiber was completely aligned with the first (1) principal direction, the components of orientation would be  $a_{11}=1.0$  and  $a_{22}=a_{33}=0.0$  [10].

$$\begin{bmatrix} \mathbf{a_{11}} & a_{12} & a_{13} \\ a_{12} & \mathbf{a_{22}} & a_{31} \\ a_{13} & a_{23} & \mathbf{a_{33}} \end{bmatrix} \quad (2.5)$$

When determining the components of the FOT of a composite, it is important to determine the fiber orientation through the thickness of the material. The fiber orientation can vary from the top surface to bottom surface of the material sample depending on the in-mold flow behaviour. In order to discuss and analyze these differences, the sample area section is split into “bins” through the thickness, illustrated in Figure 2-7. Each of these bins is treated as a separate area, and the FOT is calculated for each one. After the FOT has been found for each bin, the differences can be discussed, and trends can be found.

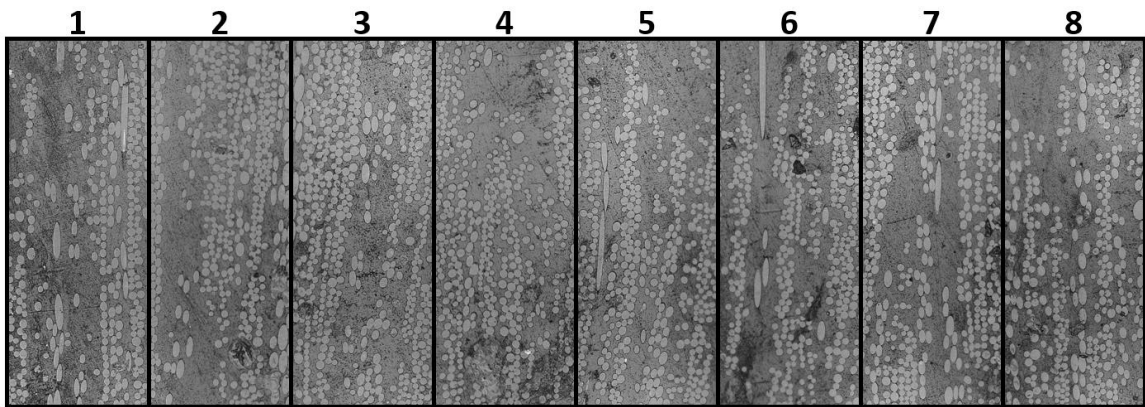


**Figure 2-7 Example of Imaged Material Split into Eight Bins**

For this study,  $a_{11}$  is parallel to the width of the sample,  $a_{22}$  is parallel to the height of the sample, and  $a_{33}$  is parallel to through the thickness of the sample (see Figure 2-8).



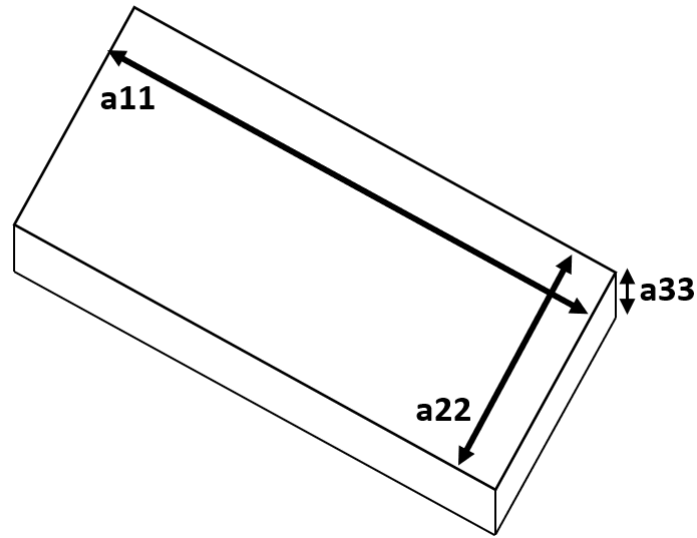


**Figure 2-8 Fiber Orientation Coordinate Convention**

The two methods for obtaining fiber orientation data to be discussed are Method of Ellipses and Micro-Computed Tomography, see Motaghi et al [11] and Buck et al [12].

### 2.5.1 Method of Ellipses

The Method of Ellipses is a destructive, but simple method. The part that is being investigated is cut along a plane and polished, then imaged with a microscope. The fibers that have been cut are now present in the plane with their cross section as an ellipse. By measuring the minimum axis, maximum axis, and angle between the major axis and horizontal, the fiber in-plane and out-of-plane angles can be calculated, as illustrated by Figure 2-9 [13].

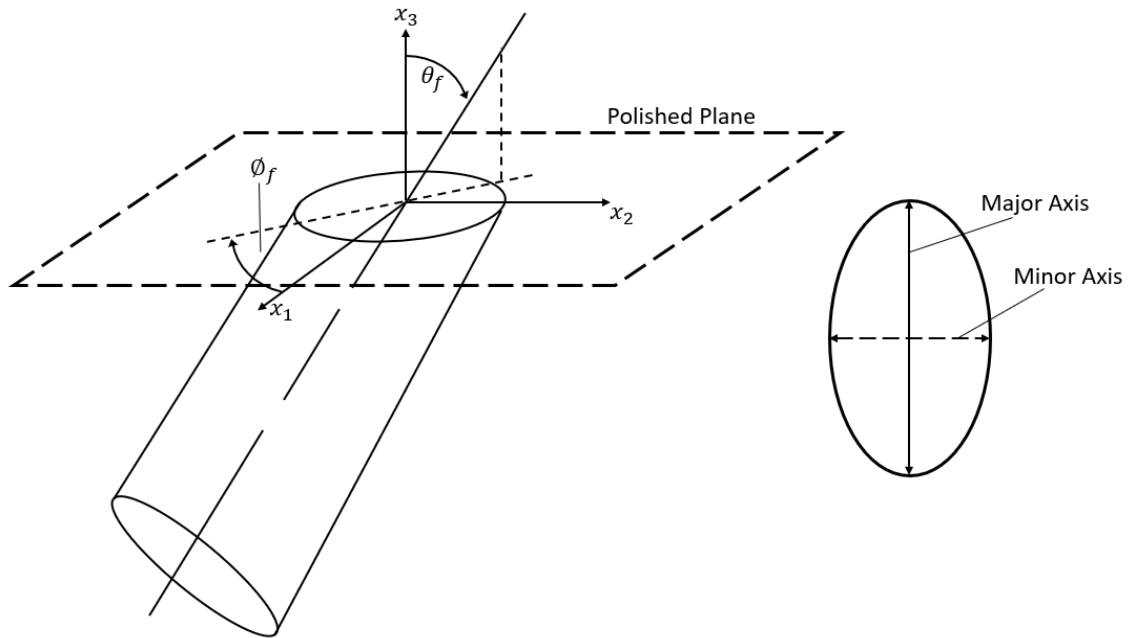


**Figure 2-9 Method of Ellipses Diagram, In-Plane Angle ( $\phi_f$ ), Out-Of-Plane Angle ( $\theta_f$ ) [Velez-Garcia, 13]**

The out-of-plane angle,  $\theta_f$ , is derived from

$$\theta_f = \sin^{-1}(\text{minor axis} / \text{major axis}) \quad (2.5.1)$$

From the in-plane and out-of-plane angles, the orientation components can be found, using the tensor below.

$$\begin{array}{ccc} a_{11} = (\sin^2 \theta_f \cos^2 \phi_f) & a_{12} & a_{13} \\ a_{12} & a_{22} = (\sin^2 \theta_f \sin^2 \phi_f) & a_{31} \\ a_{13} & a_{23} & a_{33} = (\cos^2 \theta_f) \end{array} \quad (2.5.2)$$

### 2.5.2 Micro-Computed Tomography

Micro-Computed Tomography is a method of determining fiber orientation [14]. An x-ray beam is emitted through the part and a detector captures how much of the x-ray was absorbed by the part. As dissimilar materials absorb more or less of the x-ray based on

their density (i.e., glass fibers absorb much more than a polyamide matrix), a 2-dimensional density map of the part can be made. By capturing this density map hundreds of times as the part rotates 180°, a fully 3-dimensional reconstruction of the part can be made. Figure 2-10 illustrates this process. The three-dimensional reconstruction is made using computer software and can be viewed and analyzed to determine the fiber orientation tensor of the scanned part [15]. As discussed by Sabiston et al [16] the scanning resolution is of critical importance to successful fiber orientation analysis. A lower resolution has a faster scan time, but less detail. Sabiston recommends the resolution to be no less than half of the fiber diameter. As the fibers present in Flowcore have a diameter of ~10 $\mu$ m, the scanning resolution was set to ~5 $\mu$ m/pixel.

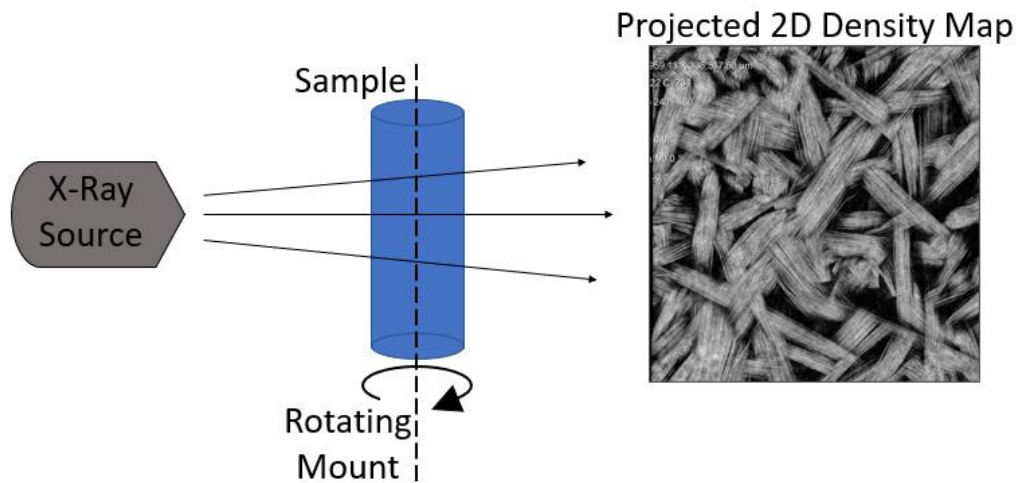


**Figure 2-10 Simplified micro-computed tomography sampling**

## Chapter 3

### 3 Experimental Characterization

#### 3.1 Flowcore Specifications

Below are the material specifications of Lanxess Tepex Flowcore [26], as provided by the manufacturer.

<b>Layup</b>	<b>According to Standard</b>	<b>Unit</b>	<b>Value</b>
Fiber	-	-	E-Glass Roving
Weaving Style	DIN ISO 9354	-	Random Mat
Area Weight (dry fabric)	DIN EN 12127	g/m <sup>2</sup>	600
Yarn	DIN EN ISO 1889	tex	30
Yarn length (nominal)	-	mm	50
Polymer	-	-	Polyamide 6 (PA6)
Fiber content (nominal)	-	vol-%	47
Thickness per layer (nominal)	-	mm	2
Laminate Density	ISO 1183-1	g/cm <sup>3</sup>	1.80

**Table 3-1 Flowcore Material Manufacturer Information**

<b>Mechanical Properties</b>	<b>Test Condition</b>	<b>According to Standard</b>	<b>Unit</b>	<b>Longitudinal</b>	<b>Transversal</b>
Tensile Modulus	23°C, ISO 1110	ISO 527-4/5	GPa	14	11
Tensile Strength	23°C, ISO 1110	ISO 527-4/5	MPa	240	190
Tensile Elongation at Break	23°C, ISO 1110	ISO 527-4/5	%	1.9	1.9
Tensile Modulus	23°C, dry	ISO 527-4/5	GPa	19	14
Tensile Strength	23°C, dry	ISO 527-4/5	MPa	260	220
Tensile Elongation at Break	23°C, dry	ISO 527-4/5	%	1.9	2.2
Flexural Modulus	23°C, dry	ISO 14125	GPa	18	14
Flexural Strength	23°C, dry	ISO 14125	MPa	450	300

**Table 3-2 Manufacturer Provided Mechanical Properties of Flowcore**

<b>Thermal Properties</b>	<b>Test Condition</b>	<b>According to Standard</b>	<b>Unit</b>	<b>Longitudinal</b>	<b>Transversal</b>
Melting Temperature	10 K/min	ISO 11357-3	°C	220	
Heat Deflection Temperature	14 GPa	ISO 75-1/-3	°C	210	
Coefficient of Linear Thermal Expansion	-35°C to 23°C, dry	ISO 11359-1.2	E <sup>-6</sup> /K	15.9	24.9
Coefficient of Linear Thermal Expansion	-35°C to 80°C, dry	ISO 11359-1.2	E <sup>-6</sup> /K	15.7	25.3

**Table 3-3 Manufacturer Provided Thermal Properties of Flowcore**

## 3.2 Manufacturing of Molded Parts

### 3.2.1 Part Types

All polymer composite parts were made at the Fraunhofer Project Center for Composites Research at Western University in London Ontario using Tepex Flowcore. For the purposes of this study, two types of parts are being considered: plaque and hat section. The plaque is a square measuring 457mm x 457mm, with a thickness of 3.5mm.

The hat section is a more complicated geometry than the plaque, while still not being as complicated as a typical full-scale production part. See Figure 3-1 for a hat section diagram.

The mechanical testing was performed on an MTS Criterion 45 Electromechanical Universal Test System, with a 200kN load cell.

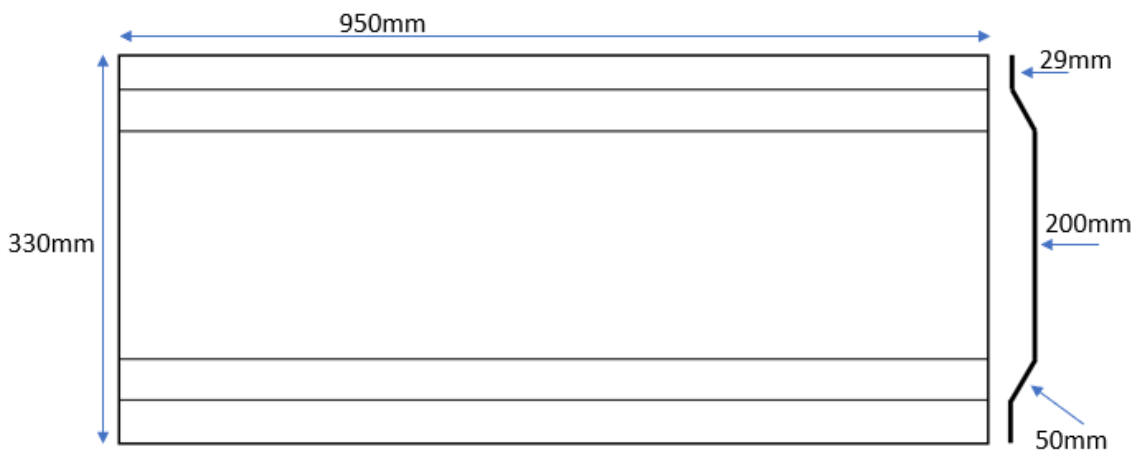


**Figure 3-1 Hat Section Diagram, Top Down (Left), Profile (Right)**

### 3.2.2 Molding Conditions

The Flowcore material was cut into blanks of various sizes depending on the mold type and how much material flow was desired. For the plaques, initial charge mold coverage was 62.4%, 90%, and 100%. The blanks were cut from 2mm or 3mm sheets of Flowcore and heated at 300°C for 16 minutes. If multiple sheets of Flowcore were needed to fill the volume of a part, they were stacked in the mold after heating. For this study, the only

molded parts with stacked sheets are the plaques with 62.4% charge coverage. The mold closed with a pressure of 300 bar and a force of 6271kN. The mold temperature was kept at 150°C and held closed for 60 seconds. For the hat sections, the charge coverage was 100%, cut from a 2mm sheet of Flowcore, and heated at 300°C for 12 minutes. The mold closed with a pressure of 500 bar and a force of 15720kN. The mold temperature was kept at 150°C and held closed for 480 seconds. See Table 3-4 for a full breakdown of molding conditions.

Xu [17], provides information on the selection of heating temperature, heating time, mold temperature, and mold-close time, as they were discovered to be important process variables. Xu also discovered a slight alignment of fiber orientation in the prefabricated material blanks, presumed to be aligned with the fabrication machine direction. This fabrication machine direction was always aligned with the molding flow direction during compression to ensure consistency.

Part Type	Initial mold coverage (area%)	Charge Dimensions (mm)	Sheet Thickness (mm)	Sheet Count	Heating Temp (°C)	Heating Time (min)	Mold Temp (°C)	Mold Closed Time (sec)	Mold Pressure (bar)	Mold Force (kN)
Plaque	62.4	457x285	3	2	300	16	150	60	300	6271
Plaque	90	457x411	2	1	300	16	150	60	300	6271
Plaque	100	457x457	2	1	300	16	150	60	300	6271
Hat Section	100	930x305	2	1	300	12	150	480	500	15720

**Table 3-4 Molding Conditions of Plaque and Hat Section**

### 3.2.3 Sample Preparation

Samples were cut from the molded parts using a waterjet cutter located at the Fraunhofer Project Center. To ensure standardized testing and results, all samples were dried for at least 12 hours at 80°C before testing, as is the standard practice for polyamides [18].

### 3.3 Fiber Length Measurements

Thomas Chang [27] developed this method while working on the parallel study to this work. Fiber length measurements were taken using 15 samples: 5 unmolded blanks, 5 plaques, and 5 hat sections. The dimensions of the fiber length measurement samples were 150mm by 150mm. These dimensions were chosen based on the work of Dahl et al. [8] who recommend sample size be 3 times as large as the maximum expected fiber length, to ensure that the fibers at the center of the sample have not been cut during the preparation. The sample is then placed in a 565°C oven for 30 minutes, which burns off the matrix completely, as shown in Figure 3-2.

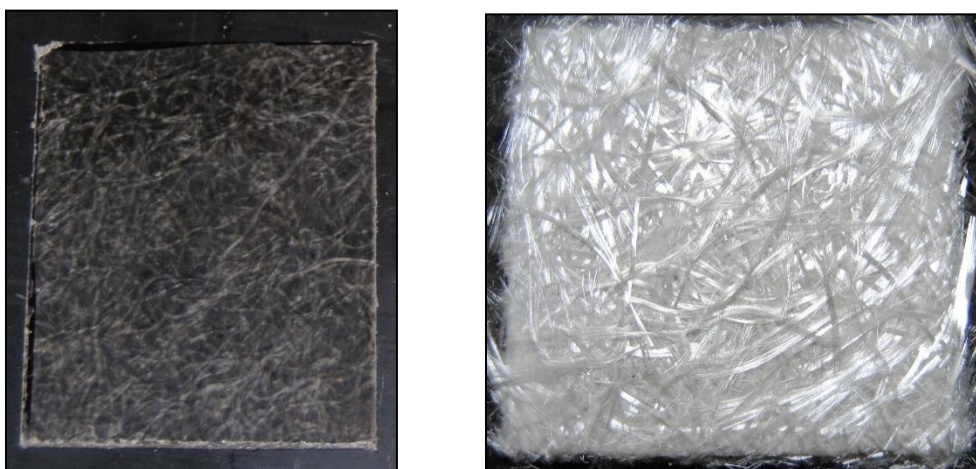


**Figure 3-2 Example of Matrix Burn Off, Before (Left) and After (Right)**

Due to the considerable number of fibers in a 150mm square, a down sampling step was necessary. Dahl uses an epoxy plug applied to the center of the sample to accomplish this, but with the basic geometry found in this study, simply using tweezers was sufficient. After the fibers had been down sampled, they were dispersed on black construction paper, as it provides a high contrast. A ruler was also placed onto the construction paper to provide a scale, then a photo was taken of the paper, ruler, and fibers (Figure 3-3). Each sample had 20 photos taken, adding up to ~6,000 fibers across the 15 samples. Using Cochran's sample size formula [28] as shown in Equation 3.3, using 6,000 fibers as the sample population ( $n_0$ ) solves for a 3.4% margin of error ( $e$ ) at a 99% confidence interval ( $Z$ ), where the estimated relevant population is 100% ( $p, q$ ).



$$n_0 = \frac{Z^2 \times p \times (1-q)}{e^2} \quad (3.3)$$

$$n_0 = 6000, z = 2.58, p = 1, q = 0$$



**Figure 3-3 Imaged Fibers for Length Measurement (Cropped)**

The images were processed using ImageJ [19] and the built-in ‘Measure’ tool (Figure 3-4), which generated a table of fiber lengths for each image after each fiber was traced by hand. The data was collated and processed in Microsoft Excel.

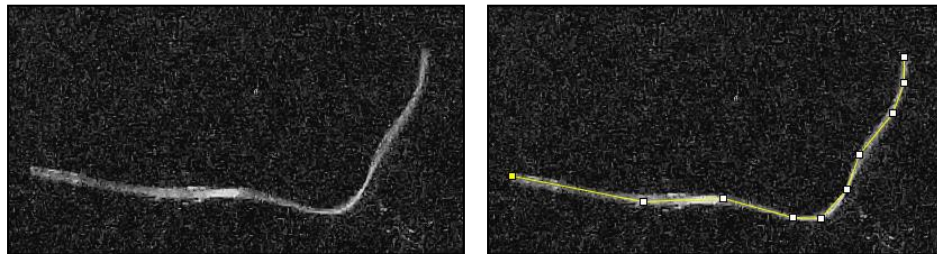


**Figure 3-4 Using ImageJ 'Measure' Tool to Follow the Fiber Curve**

### 3.4 X-Ray Micro-Computed Tomography

The micro-computed tomography testing comprised the bulk of fiber orientation characterization, with 110 samples being tested. Locations of uCT samples can be found

in Appendices B-D. The scans were performed on a Zeiss Xradia 410 Versa Micro-CT at Surface Science Western, with a resolution of 5.101 $\mu$ m per voxel, which is approximately half the fiber diameter of 10 $\mu$ m.

A novel technique for the scanning was developed, which allowed for up to 10 samples to be scanned at once. A standard uCT sample is a rectangular prism of material, typically 10mm wide by 30mm tall, and the thickness being determined by the part geometry. The technique developed was to use multiple discs of material, roughly 11mm in diameter, with the thickness determined by part geometry. See Figure 3-5 for a comparison of the two sample types.

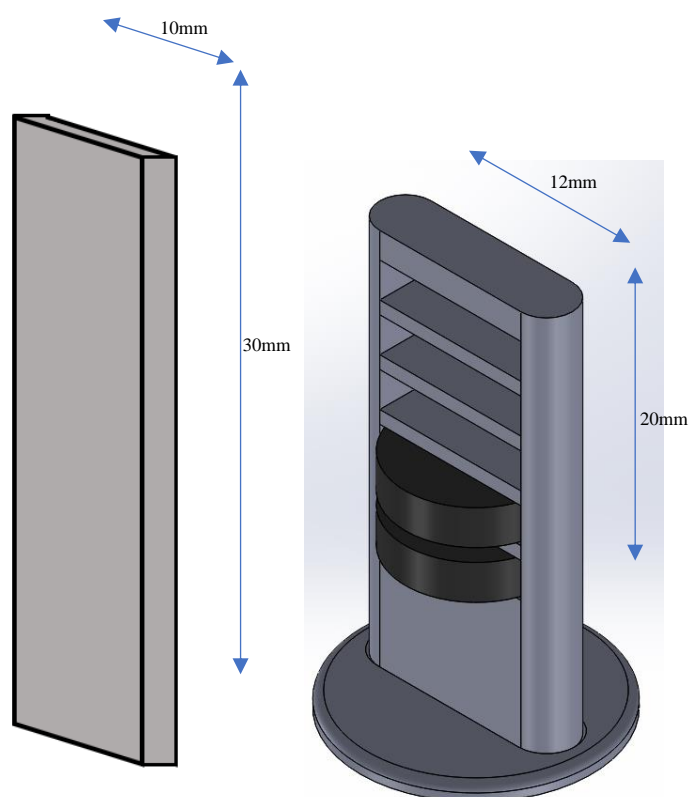


**Figure 3-5 Standard uCT Sample (Left) vs Stacked Disc Samples (Right)**

Using discs allows for a consistent x-ray intensity, as the x-ray is always travelling through 11mm of material. Additionally, the Zeiss Xradia scanner can move vertically mid-scan, stitching the multiple scans together automatically. Coupling the vertical stitching with stacking the discs horizontally allowed for up to 10 samples to be scanned in the same amount of time as 1 standard sample. The discs were held in place with a 3D

printed jig. After scanning, the scan was processed using ImageJ [19] to split the scan of 10 samples into individual files, one for each sample (Figures 3-6 and 3-7).



**Figure 3-6 Slice of uCT Scan of 10 Samples**

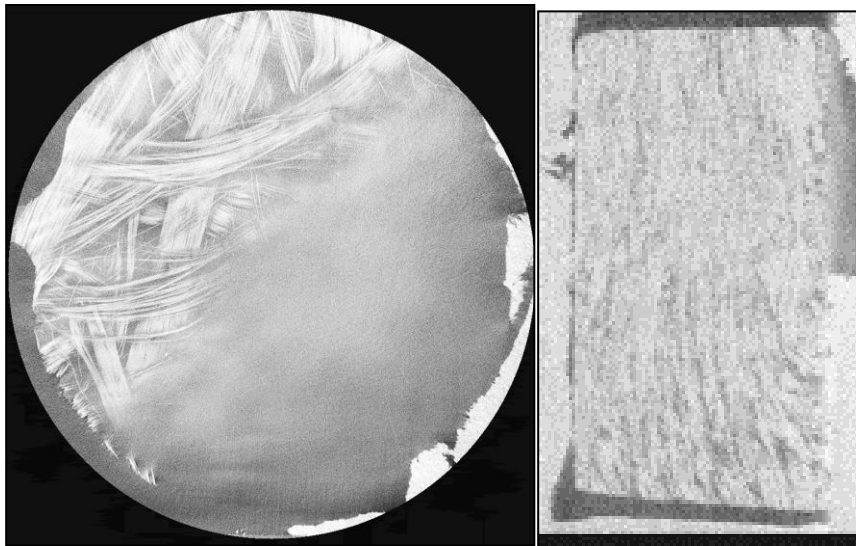


**Figure 3-7 uCT Scan of Individual Sample Pre-Alignment**

The individual files were then aligned along the x, y, and z-axes (Figure 3-8). After segmentation and alignment, Trevor Sabiston at the University of Waterloo analyzed the samples [2018] to obtain the fiber orientation distribution.

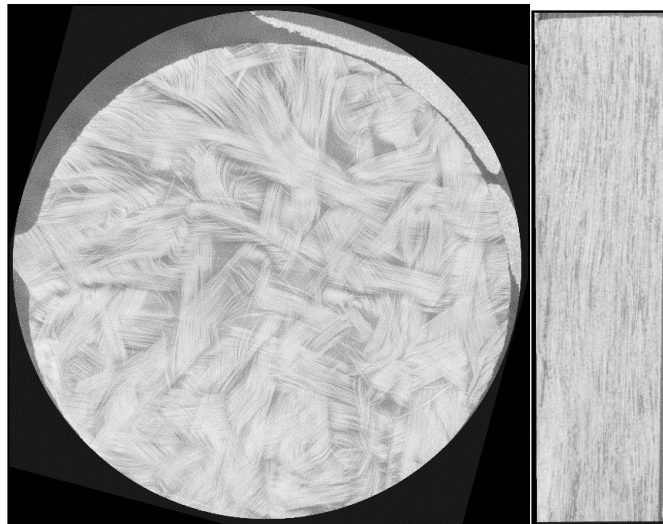


**Figure 3-8 uCT Scan of Individual Sample Post-Alignment**

### 3.5 Microscopy

Microscopy work was primarily done as a validation of uCT work. 10 uCT samples were selected at random from both the plaque and hat sections to be analyzed with both uCT and microscopy. After the samples went through the Zeiss Xradia uCT scanner, they each followed the following procedure to prepare them for imaging:

- Cut in half to expose a through-the-thickness slice
- Mounted in epoxy
- Polished
  - 3-micron diamond powder and mineral oil – 12 minutes
  - 0.25-micron diamond powder and mineral oil – 12 minutes
  - 0.05-micron aluminum oxide powder and water – 1 minute
- Cleaned with water and ethanol wipe
- Plasma etched

The samples were then imaged on a Keyence VHX-6000 Digital Microscope located at Surface Science Western at 200x magnification, using the built-in stitch function to automatically image the entire surface.

After imaging, the images were taken to ImageJ to transform them to an eight-bit image as well as rotating the image 90° before being run through a series of MatLab [21] scripts from Harrington et al [22]. The first script thresholds and binarizes the image, based on

a set of parameters. The second script identifies the major and minor axes and angle of each fiber. The third and final script calculates the fiber orientation tensor components.

## Chapter 4

### 4 Results

#### 4.1 Mechanical Properties

The mechanical properties of the material provide information to the simulation validation, but also to determine the effect of different molding conditions on the material, including any inherent anisotropy. Two types of tests were run, a tensile test and a three-point bending test, following ASTM standards D638 [23] and D7264 [24], respectively. Details can be found in Chapter 2.2.

The values for tensile stress and strain given by Lanxess, in Chapter 3.1, were confirmed and as such are not discussed further in this chapter.

##### 4.1.1 Plaque

Initial mechanical tests were run using molded plaques, measuring 457mm by 457mm with a charge coverage of ~100%. Three different molding conditions were used where the heating time of the charge was varied: 12 minutes, 16 minutes, and 20 minutes in a 300°C oven. All other molding conditions stayed constant. No significant difference in Young's Modulus due to heating times was found, as shown in Figure 4-1, so all molding trials moving forward were done with a 12-minute heating time. The samples for this heating time comparison came from 30 samples across 3 plaques, seen in Figure 4-2.

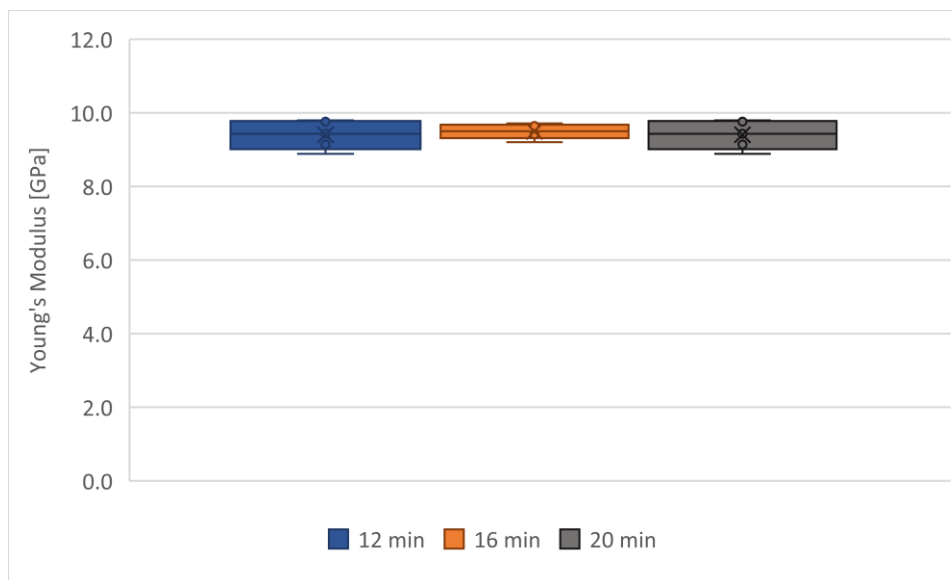


**Figure 4-1 Effect of Heating Time on Young's Modulus in 100% Coverage Molded Plaques**

The orientation of the mechanical testing sample was found to be very significant on mechanical properties, as shown in Figure 4-3 indicating that the material is anisotropic. Three different orientations were tested and can be seen in Figure 4-2: 0° (parallel to machine direction), 90° (perpendicular to machine direction), and 45°. Samples were taken from 3 different plaques and from 5 locations within 1 plaque, to reduce part-to-part and within-part error, respectively. Initially two sizes of tensile and flexure test samples were tested, as well as impact test samples. However, both the large and ASTM standard sizes produced the same material properties, but the ASTM standard sizes had a smaller standard deviation, so only the ASTM standard sizes were used going forward. Impact tests were determined to be outside the scope of this study.

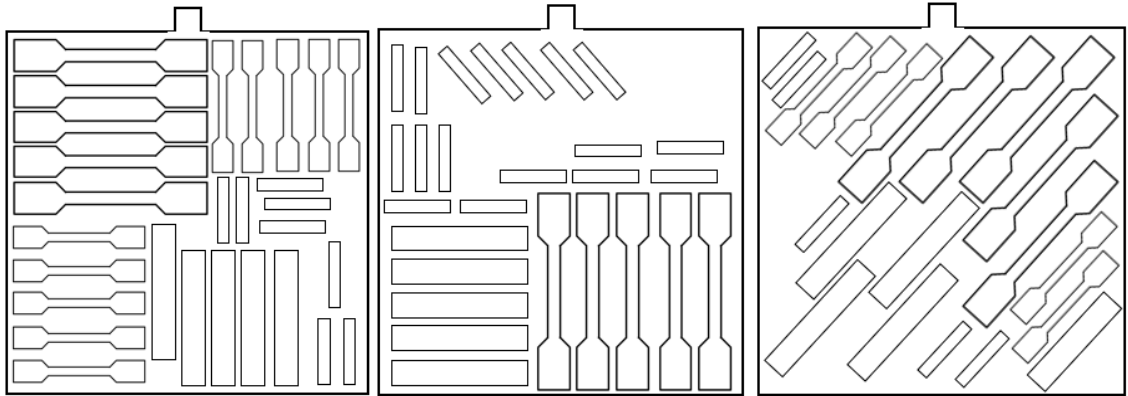


**Figure 4-2 Mechanical Test Sampling Locations in 100% Coverage Plaques**

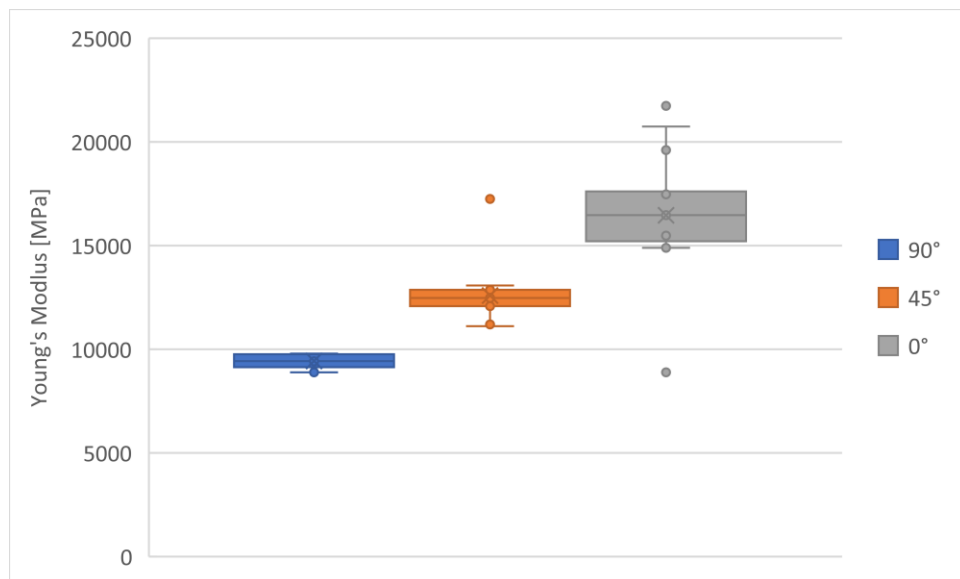


**Figure 4-3 Effect of Orientation on Young's Modulus of ST Coupons from 100% Coverage Molded Plaques**

The next investigation to be completed by mechanical testing was the effect of flow on material properties. Two molding conditions were used on the plaque mold, 62.4% initial charge coverage, and 90% initial charge coverage. Test samples were taken from areas of the plaque that experienced flow from the initial charge position to the final position, but due to the small amount of space available in the 90% coverage plaque, only test samples with a 90° orientation could be taken. Sampling locations can be seen in Figure 4-5. The mechanical properties were found to be higher on average in areas with higher flow but



not significantly, and with no significant difference between the initial charge areas of 62.4% and 90%, as shown in Figure 4-4.

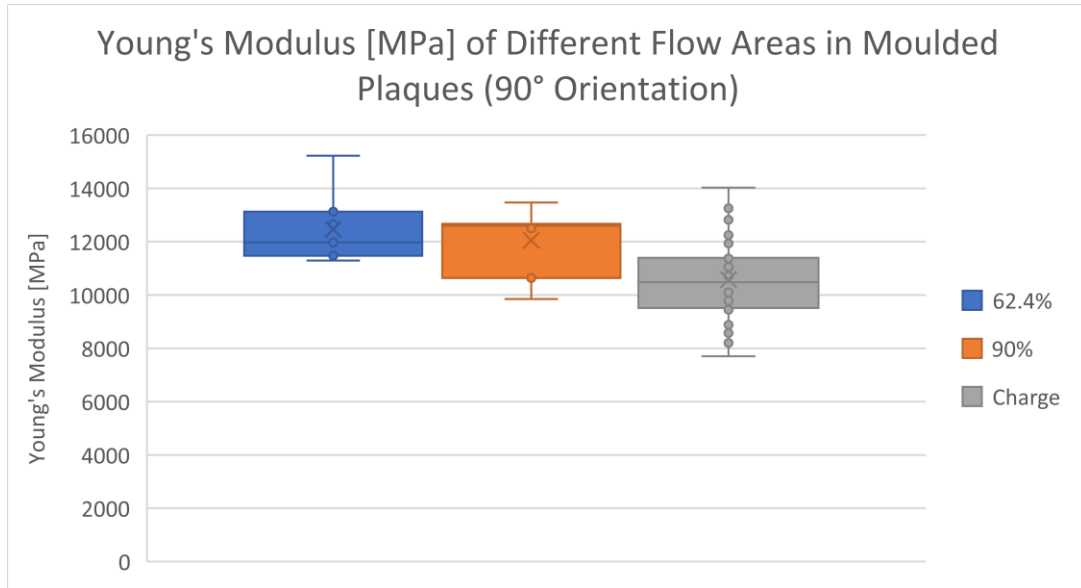


**Figure 4-4 Effect of Material Flow on Young's Modulus**

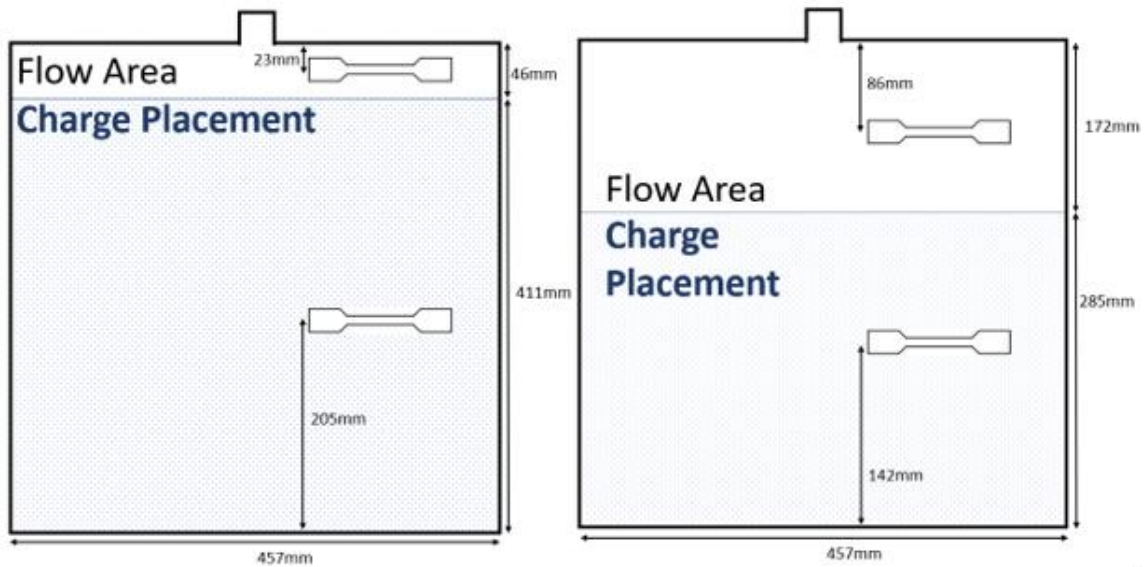


**Figure 4-5 Sampling Locations of 90° Samples for Plaques with 90% (Left) and 62.4% (Right) Charge Coverage**

### 4.1.2 Hat Section

The hat section samples were subjected to the same mechanical tests as the plaque samples to investigate if the different part geometry would affect the properties. As heating condition and high flow were found to not be significant, there were no changes in the molding conditions (i.e., 12-minute heating time and ~100% coverage). Many of the areas of the hat section geometry could only fit a 90° sample, so the bulk of the test data is perpendicular to the initial charge machine direction.

Following the same testing format as used for the plaques, 5 different hat sections were used to provide for 5 samples from each area of interest - see Figure 4-6 for the hat section labelling diagram. Due to the areas of interest being small (excluding A and B), only one sample could be taken from each area per hat section.

<b>G</b>			<b>J</b>			<b>M</b>
<b>E</b>			<b>F</b>			
<b>A</b>		<b>B</b>				
<b>C</b>			<b>D</b>			
<b>N</b>			<b>Q</b>			<b>T</b>

**Figure 4-6 Hat Section Labeling Diagram**

Analysis using single factor ANOVA tests showed that no significant difference (at xxx level) was found in mechanical properties between sample areas A, B, C, D, E, and F. Single factor ANOVA tests were used to investigate if the means of several populations were equal, as opposed to just two populations. The edge grouping of G, J, M, N, Q, and T does have significant differences compared to the central grouping (A, B, C, D, E, F). Breaking down the edge grouping further, the corner grouping (G, M, N, T) does not have significant differences between locations, and neither does the central edge grouping

(J, Q), but there is a significant difference between the corner grouping and the central edge grouping. See Figure 4-7 for the graph of corresponding values for flexural modulus.

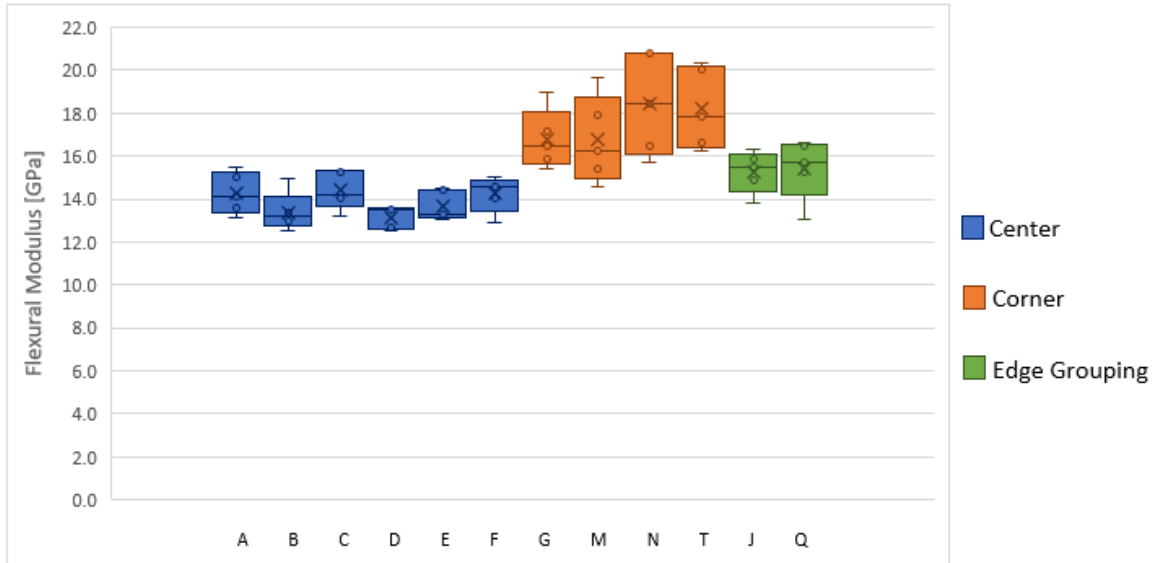


**Figure 4-7 Comparison of Flexural Modulus in Hat Section Sample Areas at 90° Orientation to Machine Direction**

The mechanical properties of the 100% coverage plaques and hat sections across all sampling areas in the 90° orientation were also compared, to determine if any significant difference of the means between the two types of parts was present. No significant difference in the means was found (Figure 4-8).

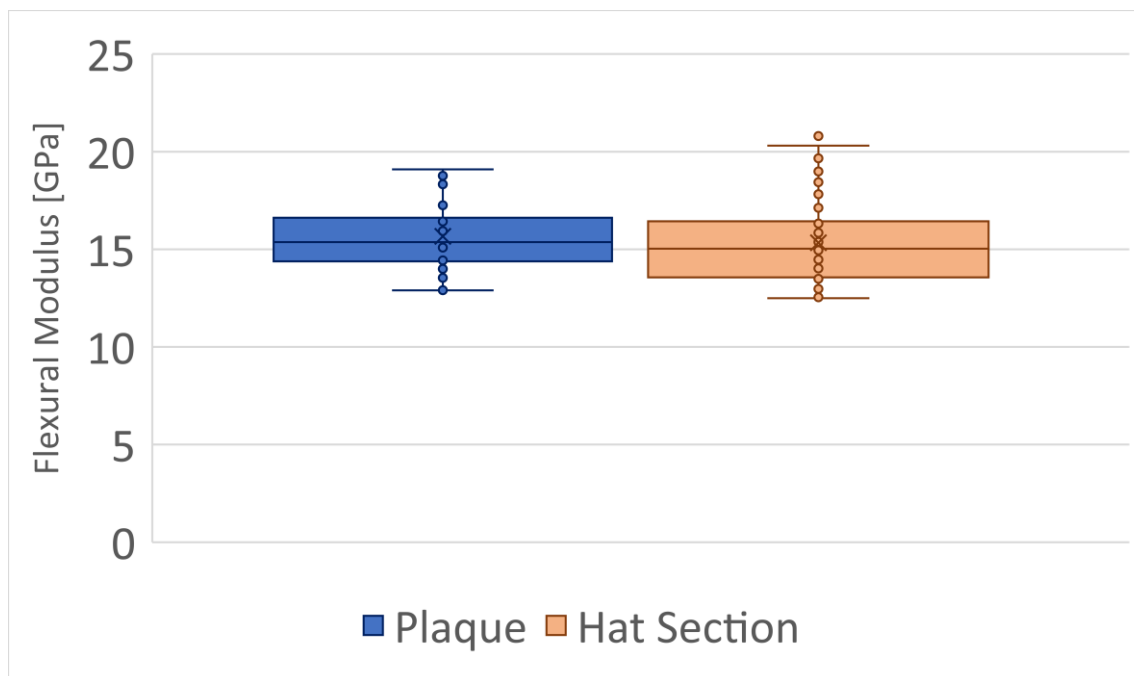


**Figure 4-8 Comparison of Flexural Modulus Between All Locations of Plaques and Hat Sections**

## 4.2 Fiber Concentration

Fiber concentration was determined using matrix burn off tests to measure weight loss. Initially, tests were conducted in a burn off oven, but a TGA was made available, and all subsequent tests were performed using it. The unmolded Flowcore was tested with burn off, while the plaque and hat sections were tested with a TGA. Three process conditions on local fiber concentration in the final part were investigated: raw material, material flow during compression, and part geometry. Lanxess Tepex Flowcore has a reported volume percentage of fibers (vol%) is 47%, which in turn can be calculated as a weight percentage (wt%) of 66.32%.

### 4.2.1 Fiber Concentration in Source Material

Across 5 samples from 3 sheets of unmolded Flowcore, the mean fiber concentration was found to be 66.95 wt% with a standard deviation of 1.07, in agreement with the reported Lanxess Tepex Flowcore information.

#### 4.2.2 Effect of Flow on Fiber Concentration

To determine the effect of compression flow on fiber concentration, samples were taken from plaques that had a 90% initial charge area coverage and a 62.4% initial charge area coverage. Schematics of sample locations are shown in Figure 4-9. The sampling locations differ between the plaques, as it was desired to have a sample immediately on either side of the charge placement line as well as a sample at the maximum flow length. The rest of the samples were evenly spaced out along the flow length. The rest of the samples were evenly spaced out along the flow length.

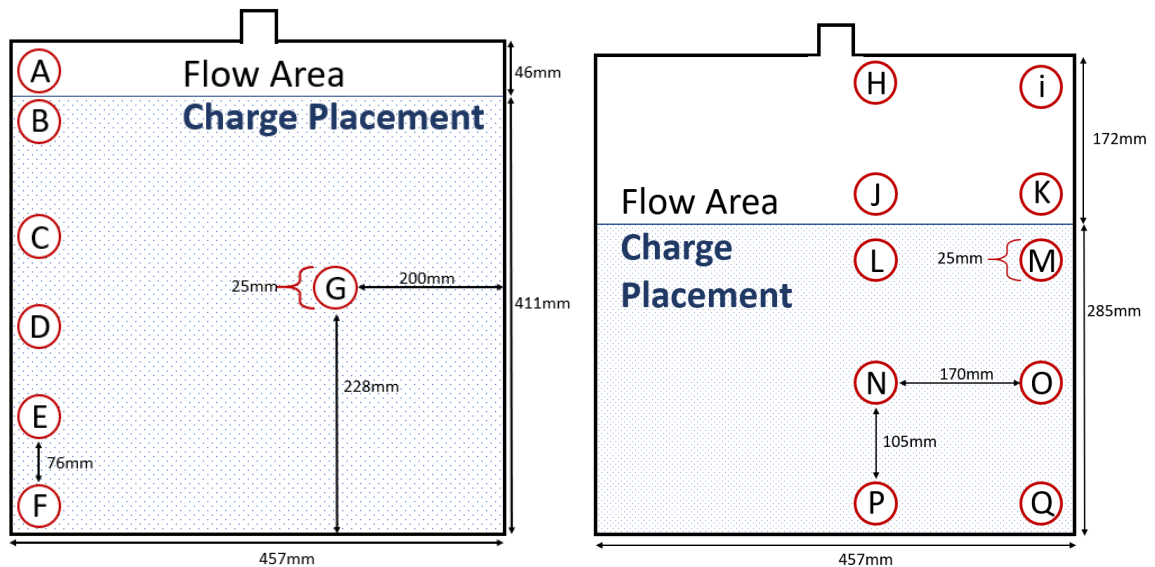


**Figure 4-9 Plaque Concentration Sampling Diagram for 90% Charge Coverage (Left) and 62.4% Charge Coverage (Right)**

Both the 90% and 62.4% charge coverage plaques were found to have lower fiber concentrations than the unmolded material at all locations (Figure 4-10). However, the sampling locations at the end of the flow paths had no significantly higher or lower concentrations than anywhere else in the plaque, and the standard deviation across all sampling locations was low, with 0.94 for the 90% coverage and 1.23 for the 62.4% coverage. This indicates that the drop in fiber volume percent is only due to the act of molding, a claim backed up by the results in 4.2.3 and the work of Thomas Chang [27].

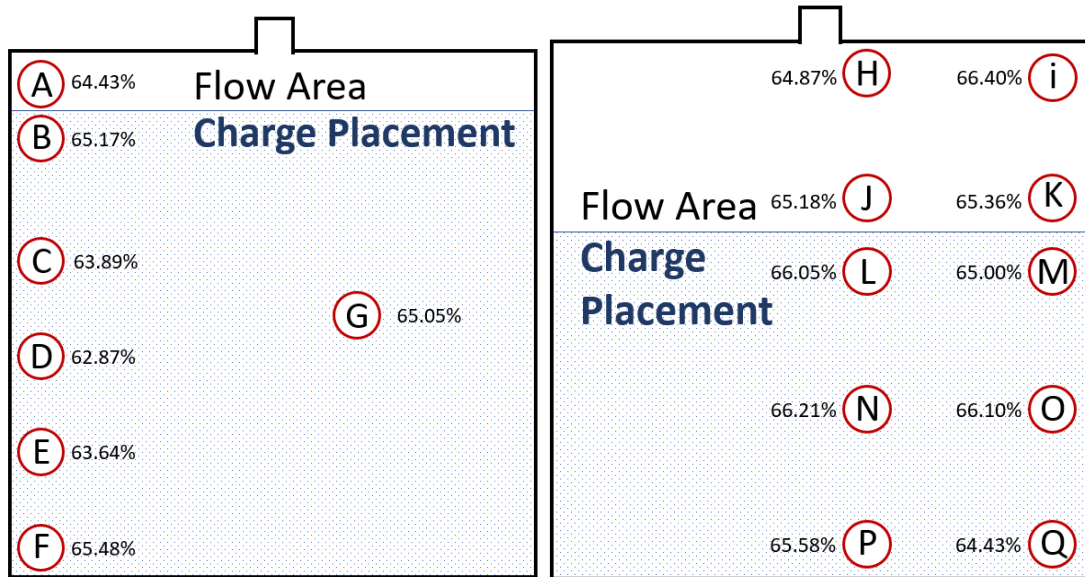


**Figure 4-10 Fiber Weight Percent Throughout Plaques with 90% (Left) and 62.4% (Right) Charge Coverages**

		Fiber Weight %	Average	Std Dev
90%	A	64.43	64.36	0.94
	B	65.17		
	C	63.89		
	D	62.87		
	E	63.64		
	F	65.48		
	G	65.05		
62.40%	H	64.87	65.12	1.23
	I	66.40		
	J	65.18		
	K	65.36		
	L	66.05		
	M	65.00		
	N	66.21		
	O	62.10		
	P	65.58		
	Q	64.43		
Unmolded	1	68.04	66.95	1.07
	2	66.59		
	3	65.53		
	4	66.59		
	5	68.00		

**Table 4-1 Fiber Weight Percent of Plaques and Unmolded Samples**

### 4.2.3 Effect of Part Geometry on Fiber Concentration

Six locations across 5 different hat section parts were investigated to observe the effect of part geometry on fiber concentration. Referencing Figure 4-12, the sample locations used were A, B, E, F, G, and J.

Similar to the results found with the plaques, fiber concentration across the entire hat section was found to be lower than the unmolded Flowcore, except for location G, the corner location. The corner location has a higher fiber concentration due to the flow cessation at the corner, leading to the fibers accumulating. Even though there was a higher concentration of fibers at location G, it has a negligible effect on the material properties, which are discussed in section 4.1.2. Location G also has a very high standard deviation of 7.16. Location E also has a higher average weight percent than the other locations but is below the unmolded weight percent of 66.95% provided in Table 3-1 and falls within the standard deviation of the other locations. Concentrations for all locations can be found in Figure 4-11. These findings indicate that simple part geometry has little effect on the fiber concentration but molding the material does result in a slight decrease of local fiber weight percent.

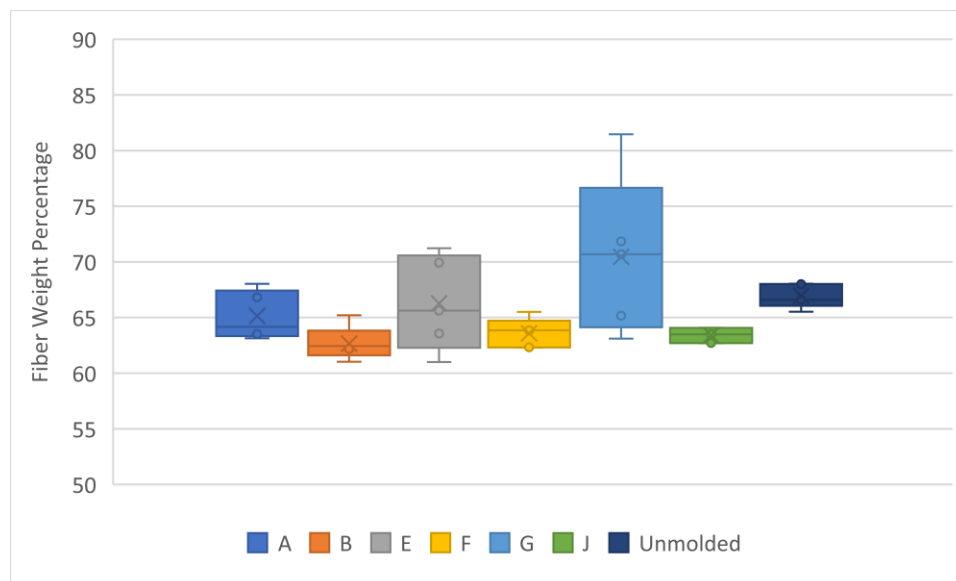


**Figure 4-11 Hat Section Fiber Weight Percent Graph**





sections. Sampling locations of the molded parts can be seen in Figures 4-13 and 4-14. Five samples of each type were tested, with ~6,000 fibers being measured. As is shown in both Table 4-3 and Figure 4-15, 88.78% of the fibers were in the range of 46mm to 54mm, with the average fiber length being within one standard deviation of 50mm for all three sample types

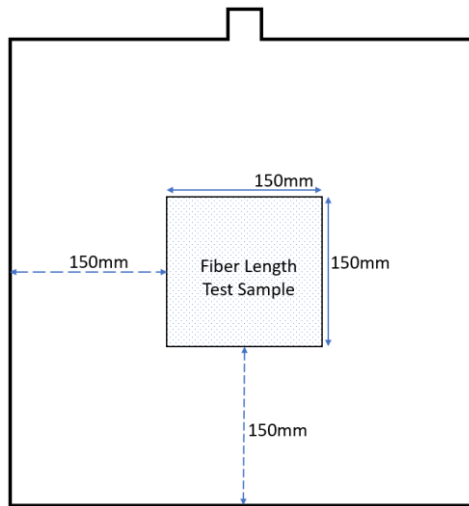


**Figure 4-13 Fiber Length Test Sample Location: Plaque**

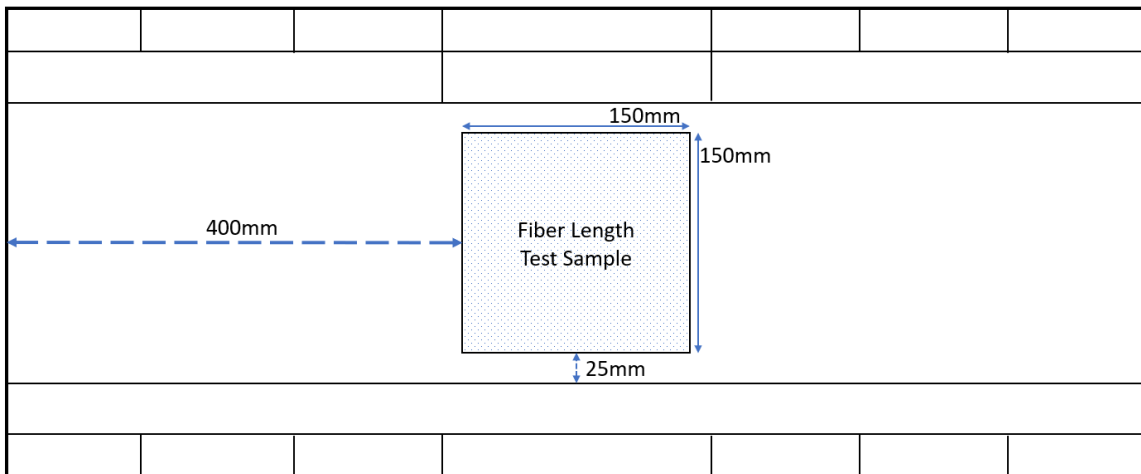


**Figure 4-14 Fiber Length Test Sample Location: Hat Section**

	Unmolded	Plaque	Hat Section	
Between 46.1mm and 52.0mm	74%	74%	79%	% of total fibers
	50.0	49.7	49.5	average length [mm]
Between 46.1mm and 54.0mm	91%	86%	90%	% of total fibers
	50.5	51.6	49.9	average length [mm]

**Table 4-3 Results of Fiber Length Measurements**

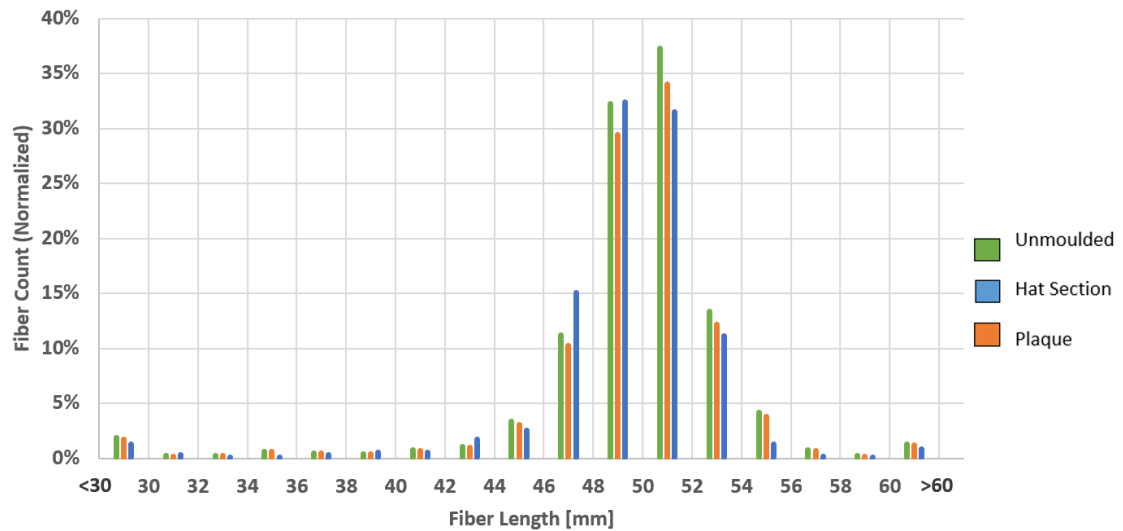


**Figure 4-15 Fiber Length Distribution Graph of Unmolded Sheets, Plaques, and Hat Sections**

### 4.4 Fiber Orientation

For the normalized thickness of the orientation diagrams, 0.0 is the bottom of the sample and 1.0 is the top, which is also the top of the mold.

The sample naming convention is a letter followed by a number. The letter indicates part type as shown in Table 4-4, and the number can be referenced in the appendix to find the sample location and molding conditions.

<b>Part Type</b>	<b>Letter</b>
Unmolded	A
100% Coverage Plaque	B
90% Coverage Plaque	C
62.4% Coverage Plaque	D
Hat Section	E

**Table 4-4 Fiber Orientation Sample Naming Convention**

#### 4.4.1 Optical Microscopy

As noted in Chapter 3.3 and 3.4, fiber orientation was found through optical microscopy and the method of ellipses. Figures (4-16 to 4-19) show the orientation tensor components from 8 randomly selected uCT test samples that also underwent optical microscopy, as well as the averaged results. The sample numbers are indicated in the figures, and the locations for the samples can be found in Appendices B-D by referencing the sample number. The fibers are primarily planar in orientation, skewed to the  $a_{11}$  and  $a_{22}$  directions, but a clear bias for the  $a_{22}$  direction is also visible. The  $a_{22}$  direction is parallel to both the machine direction of the molded parts and the rolling direction of the unmolded sheets, so this was to be expected. The  $a_{22}$  component also has the highest standard deviation, as shown in Table 4-5, but remains further than one standard deviation away from  $a_{11}$ .

Component of Fiber Orientation	$a_{11}$	$a_{22}$	$a_{33}$
Average Across Thickness	0.3087	0.5087	0.1826
Standard Deviation	0.0363	0.0652	0.0385

**Table 4-5 Averages of Microscopy Samples Components of Fiber Orientation**

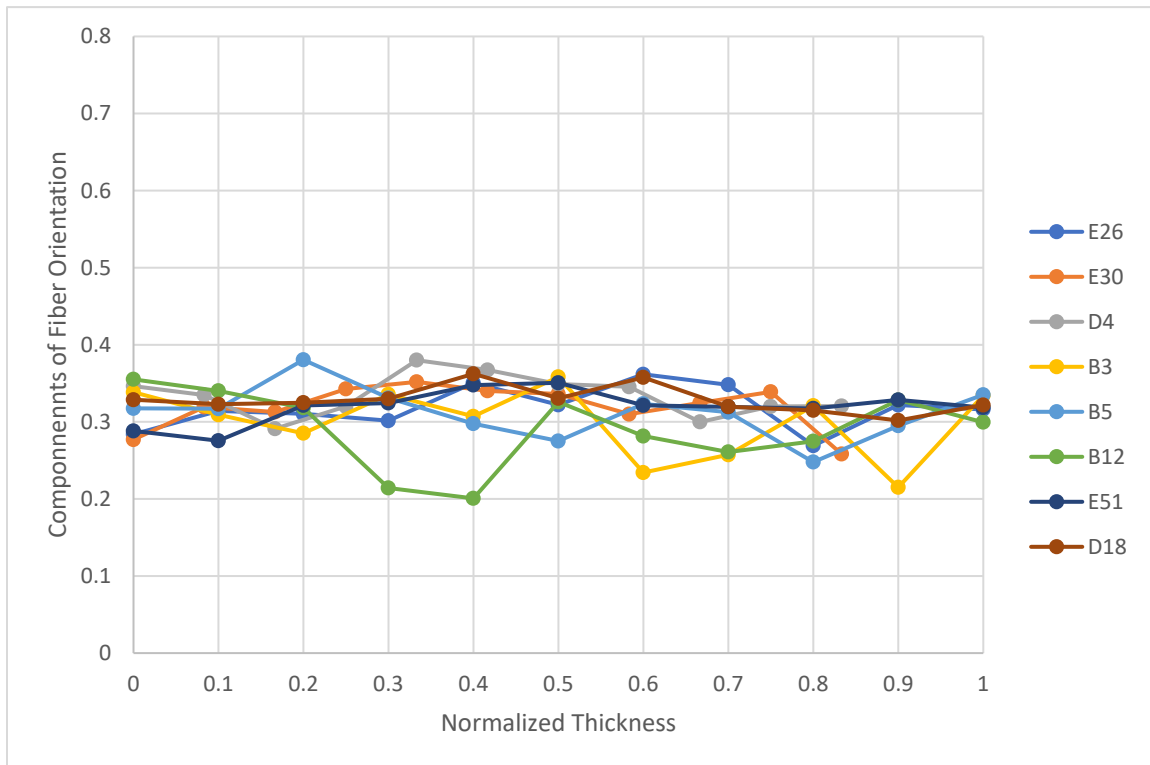


**Figure 4-16 Optical Microscopy  $a_{11}$  Orientation Compilation**

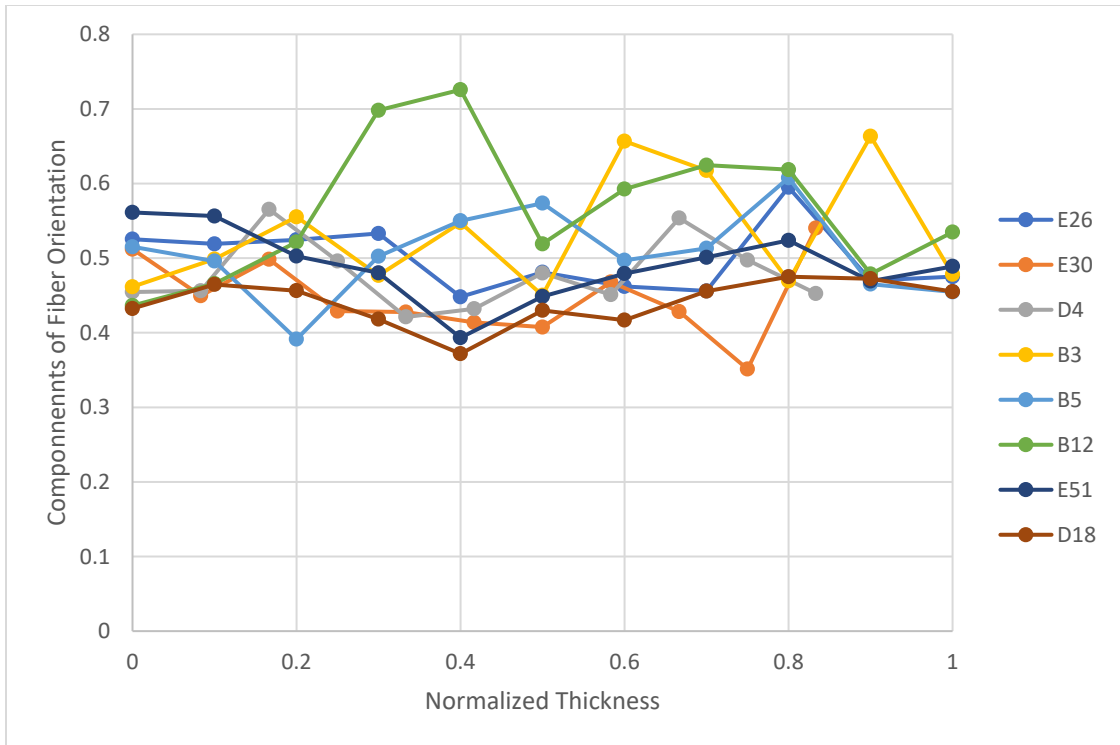


**Figure 4-17 Optical Microscopy  $a_{22}$  Orientation Compilation**

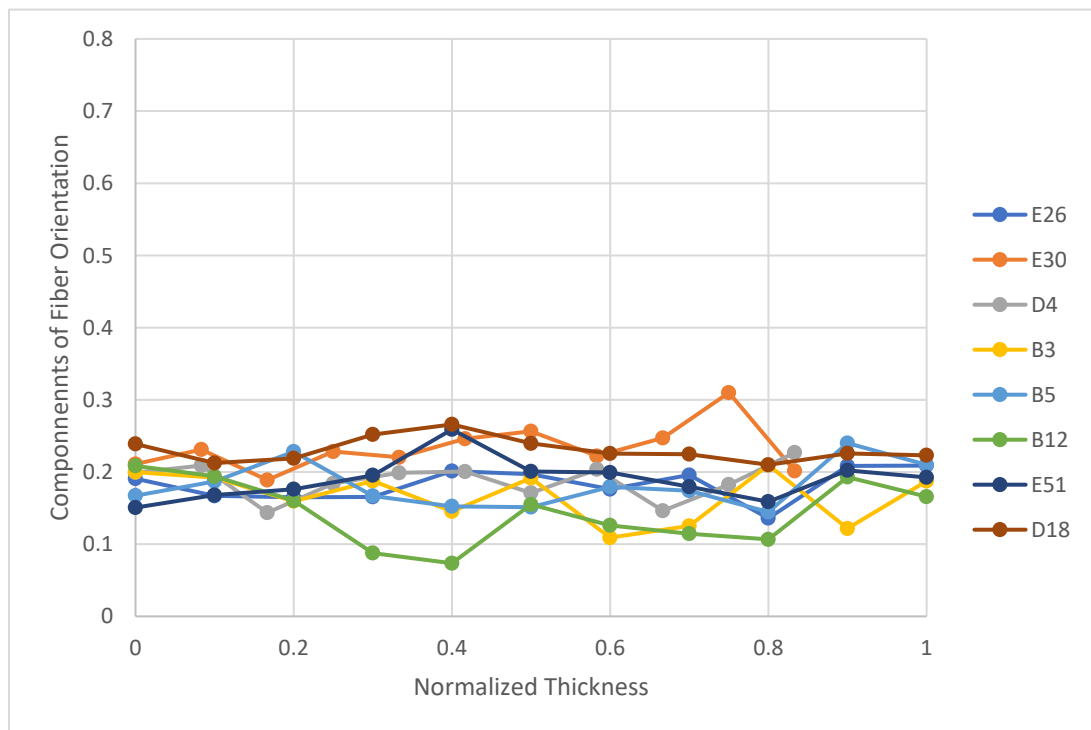


**Figure 4-18 Optical Microscopy  $a_{33}$  Orientation Compilation**

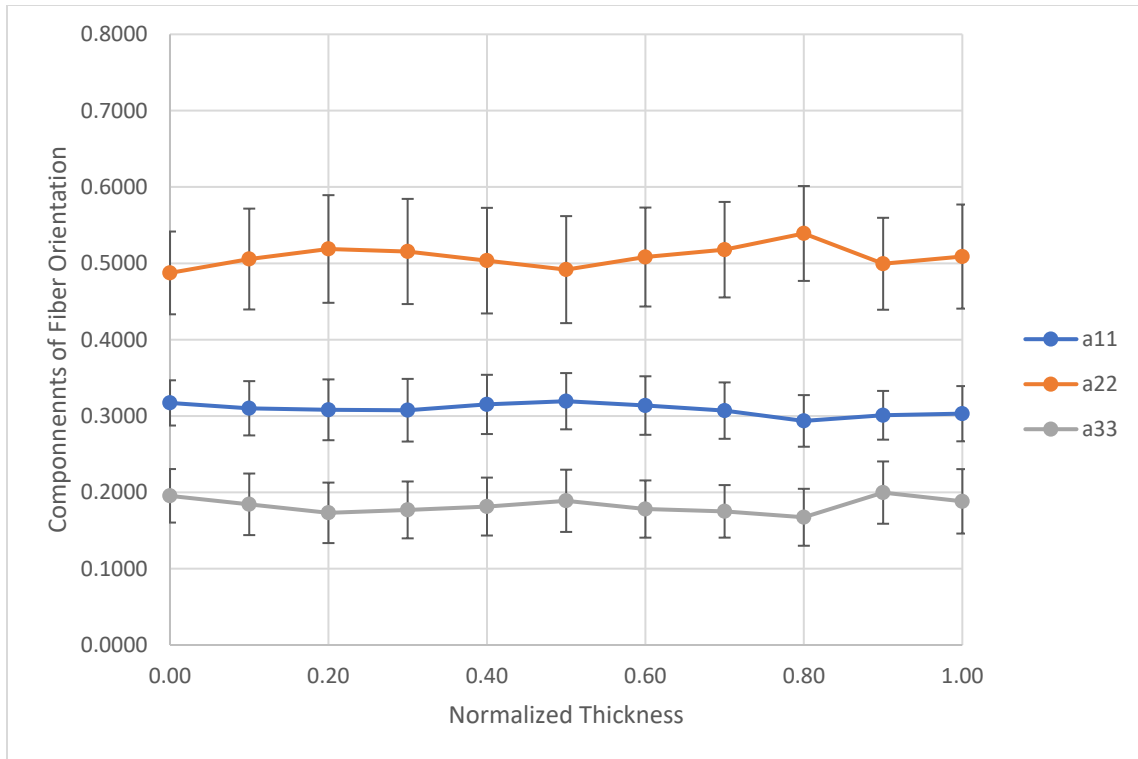


**Figure 4-19 Averaged Orientation Components of All 8 Microscopy Samples**

#### 4.4.2 Micro-Computed Tomography Validation

To validate the accuracy of the uCT fiber orientation tests, optical microscopy was used. From the pool of 110 uCT samples, 8 were randomly selected to also undergo optical microscopy testing. The 8 selected were E26, E30, D4, B33, B5, B12, E51, and D18. As shown in Figures 4-20, 4-21, and 4-22, there is agreement between the orientation tensors found using the two different methods.

There are several reasons for the few discrepancies that exist between the testing types. One difference is the number of bins taken across the sample; the microscopy samples were split into 11 bins, while the uCT samples were split into 13 bins. The MatLab code being used to run the method of ellipses on the microscopy samples, as discussed in Ch 3.5, ran much slower and would sometimes freeze entirely if more than 11 bins were used. Despite the data points being at different locations through the thickness of the samples, similar trends are clearly visible. A reason for differences in the values at the top and bottom of the sample is fiber breakage during processing. When the uCT samples

were cut in half to become microscopy samples, no matter how delicately, some of the fibers at the edge were always damaged.

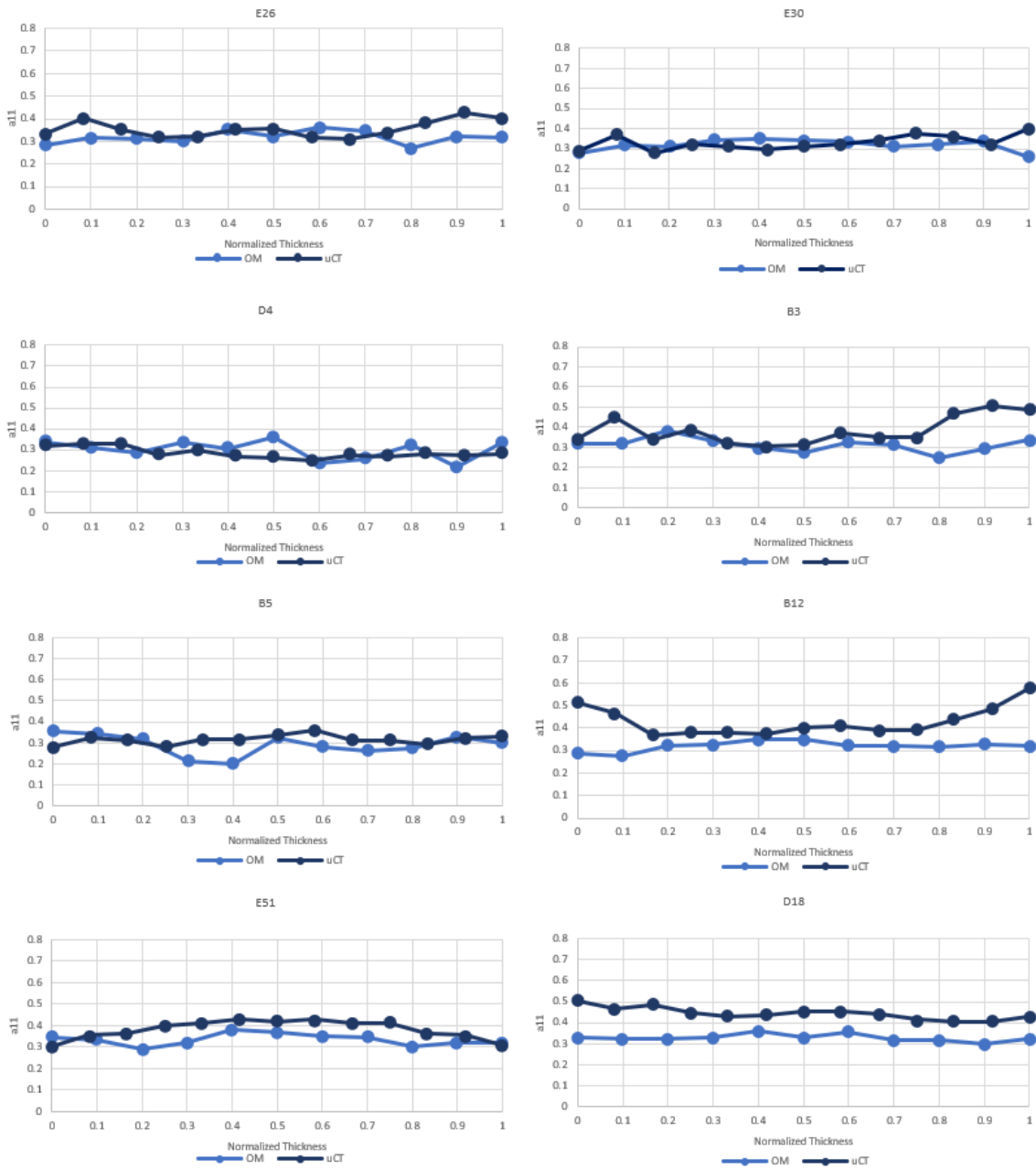


**Figure 4-20 uCT and OM Comparison of  $a_{11}$**



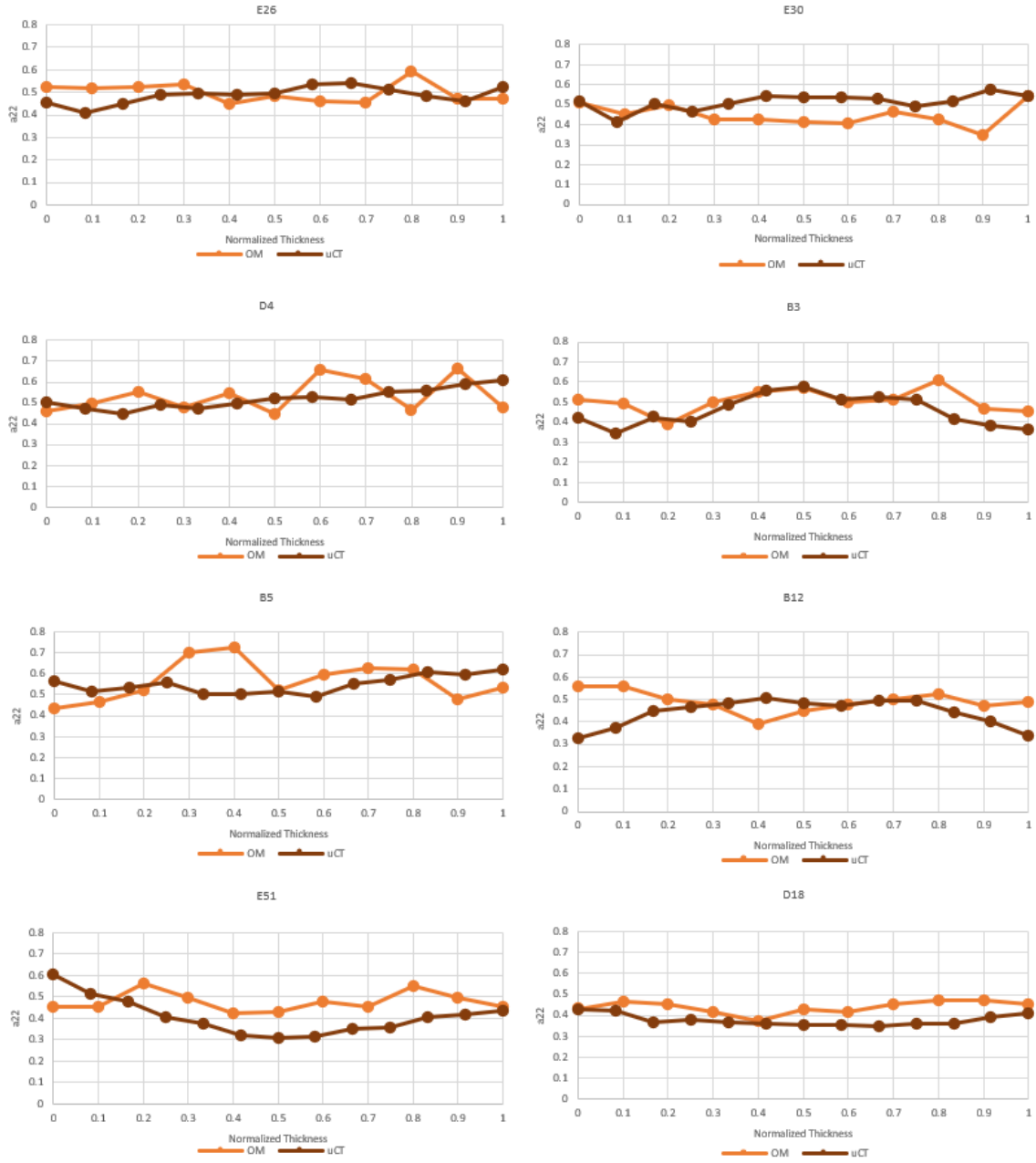
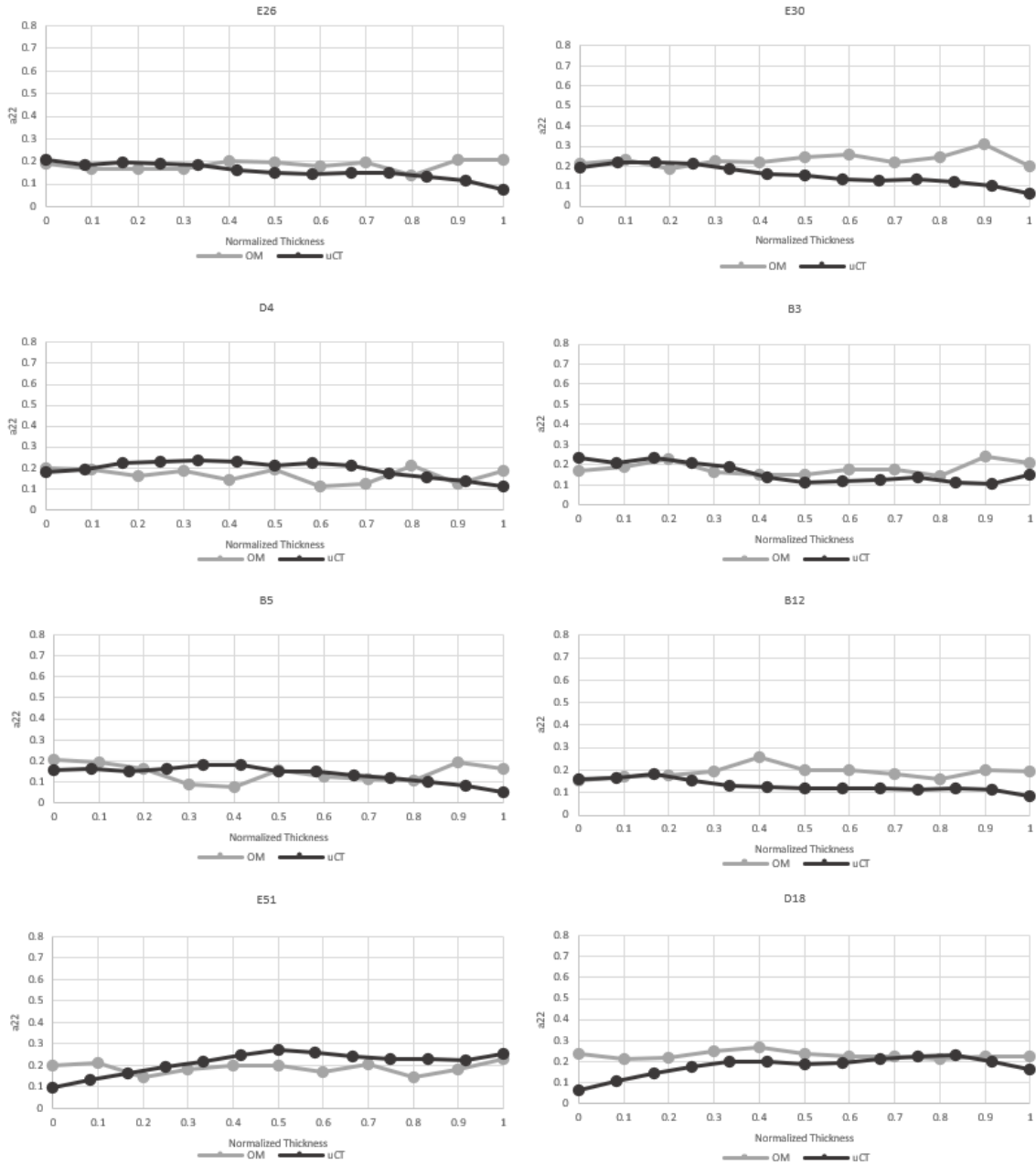


Figure 4-21 uCT and OM Comparison of a22



**Figure 4-22 uCT and OM Comparison of  $a_{33}$**

#### 4.4.3 Micro-Computed Tomography

As using micro-computed tomography to find the orientation tensor was found to be an accurate technique, all subsequent work for fiber orientation distribution was performed using uCT. 108 samples were scanned in total: 54 from 9 plaques and 54 from 8 hat sections.

### 4.4.3.1 Plaques

Three different plaque conditions were tested: 62.4%, 90%, and 100% coverage, with various sampling locations as seen in Figure 4-23. Important sampling locations are D, C, F, and B, which overlap between plaque types.

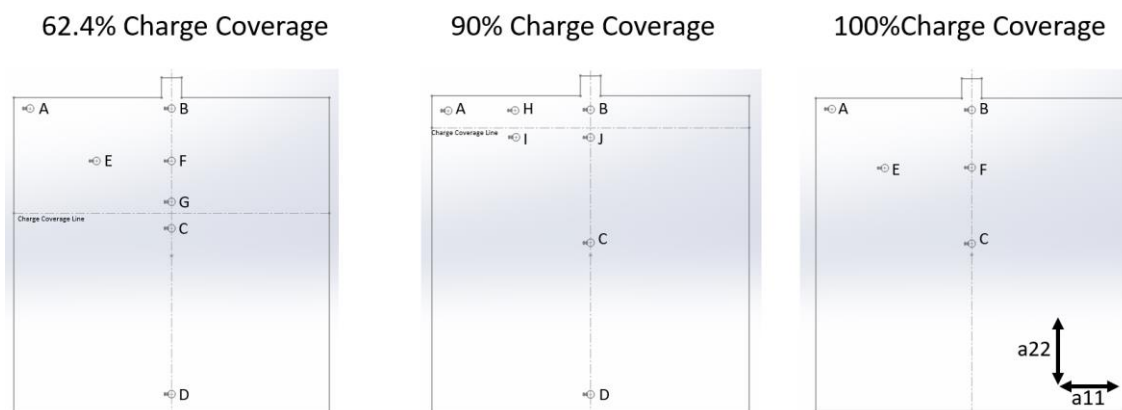


**Figure 4-23 uCT Plaque Sample Locations for Different Initial Charge Coverage**

Samples were taken to observe the effect of material flow on fiber orientation. Material flow was found to influence the observed fiber orientation distribution. Points C, B, and F from the 62.4% charge coverage plaques were examined as they are in a direct line along the flow path, with C being within the charge area, B being at the edge of the plaque, and F being between C and B. Overall, from C to B,  $a_{11}$  decreased by 0.1,  $a_{22}$  did not change, and  $a_{33}$  increased by 0.08. However, the changes from C to F were a decrease in  $a_{11}$  of 0.17, an increase of 0.09 in  $a_{22}$ , and an increase of 0.09 in  $a_{33}$ . These changes in the fiber orientation distribution can be seen in Figures 4-24, 4-25, 4-26, and the data in Table 4-6.

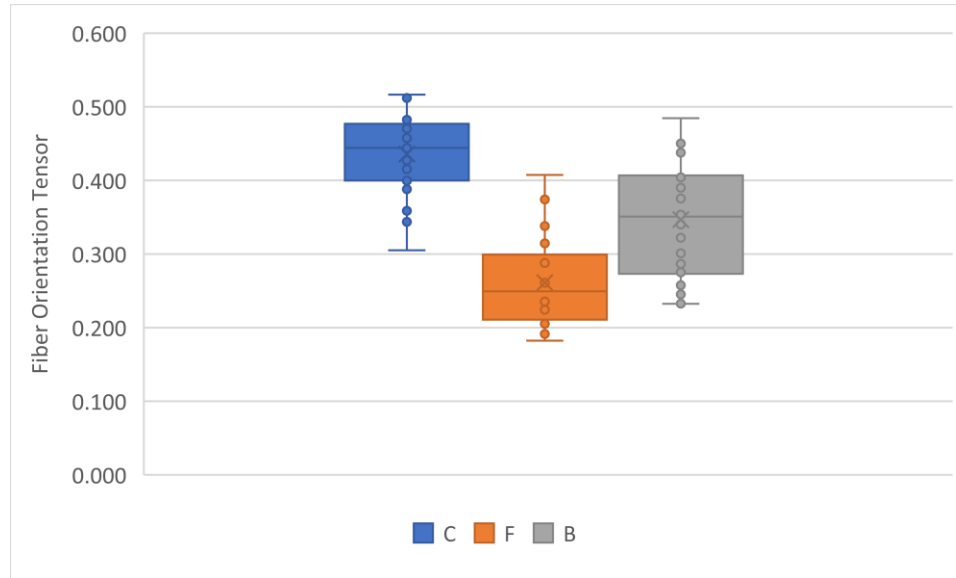


**Figure 4-24  $a_{11}$  across Locations C, F, and B of 62.4% Coverage Plaques**

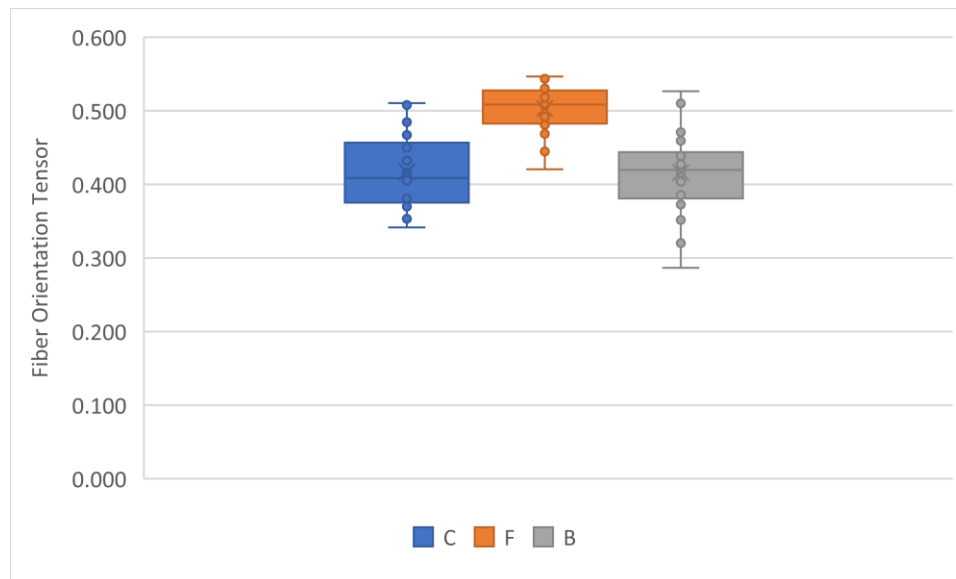


**Figure 4-25  $a_{22}$  across Locations C, F, and B of 62.4% Coverage Plaques**

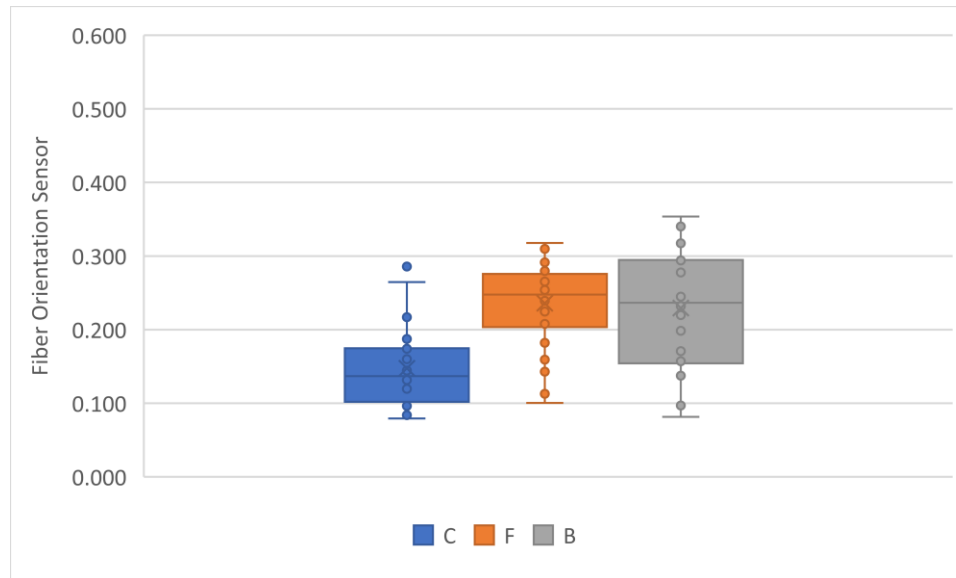


**Figure 4-26  $a_{33}$  across Locations C, F, and B of 62.4% Coverage Plaques**

	Average		
	$a_{11}$	$a_{22}$	$a_{33}$
C	0.436	0.417	0.148
F	0.261	0.503	0.236
B	0.347	0.416	0.229
	Change		
C -> F	-0.175	0.086	0.088
F -> B	0.086	-0.087	-0.007
C -> B	-0.104	-0.001	0.082

**Table 4-6 Fiber Orientation Tensor Component Changes with Flow in 62.4% Charge Coverage**

#### 4.4.3.2 Hat Sections

Part geometry was found to influence fiber orientation. The further the material is forced from the initial x-y plane, which is the plane where locations A and B can be found in the Hat Section, the higher  $a_{22}$  becomes and the lower  $a_{11}$  becomes, with no change to  $a_{33}$ .

This can be seen in areas C, E, G, and N of the hat section, when compared to area A. Through-the-thickness orientation,  $a_{33}$ , was found to have negligible change throughout the different sample locations of the hat section. As charge coverage for the hat sections is close to 100%, effects from material flow are assumed to be negligible based on the results in 4.4.3.1, making the difference in geometry an explanation for the changing fiber orientation. A possible contributor to the change in fiber orientation due to part geometry is how the charge is introduced to the mold: with the plaques the charge can be placed flat, but with the hat sections the charge must be draped over the mold geometry. The draping happens due to the flexibility of the charge at high temperatures, which is what allows it to be molded. However, the draping does stretch and deform the initial charge, which could influence the fiber orientation in addition to material flow. See Figure 4-27 for an example of the changing orientation, and Table 4-7 for detailed values.

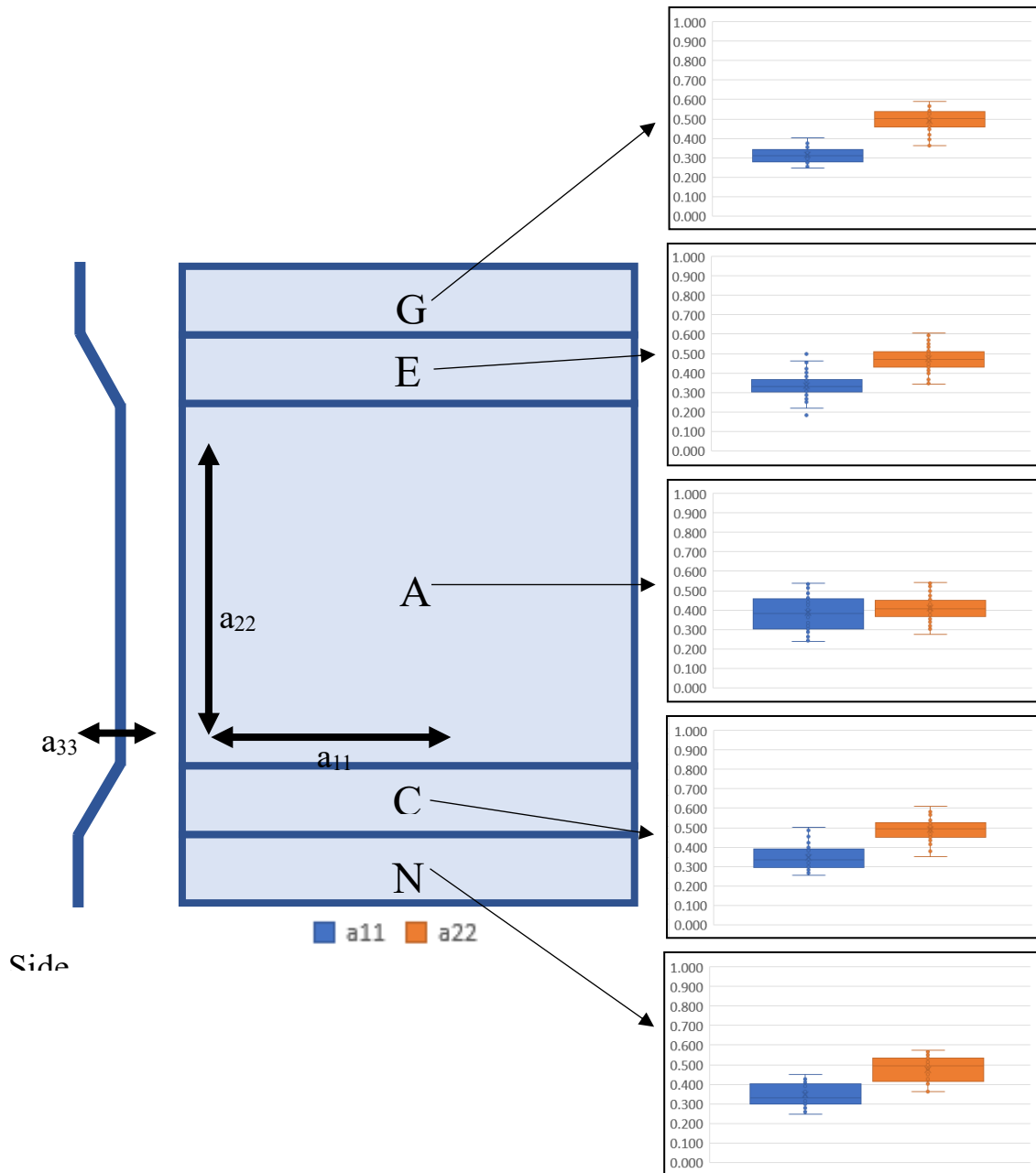


**Figure 4-27 Increase of  $a_{22}$  and Decrease of  $a_{11}$  in Hat Section Parts as Material Travels Through Z-Axis**

	$a_{11}$	$a_{22}$	
G	0.314	0.491	Top Edge
E	0.336	0.468	
A	0.386	0.410	Center
C	0.344	0.478	
N	0.345	0.475	Bottom Edge

**Table 4-7 Comparison of Average Values of Primary Components of Orientation  $a_{11}$  and  $a_{22}$  of Hat Section**



## Chapter 5

### 5 Conclusion and Future Work

Several methods, including micro-computed tomography, optical microscopy, and thermogravimetric analysis, were taken and developed to characterize the microstructure of Lanxess Tepex Flowcore, its mechanical properties, and the effects that different molding conditions and part shapes have on the microstructure and mechanical properties, including fiber orientation, fiber length, and fiber concentration.

Micro-computed tomography was used to analyze the fiber orientation, represented as fiber orientation tensor components, which can be used to validate mold-filling simulations. This study, however, only focused on the characterization.

The contribution to the field of materials engineering made by this study, outside of the data gained on a specific material, is the development of a technique for micro-computed tomography that increases the accuracy of the scans while allowing multiple samples to be scanned simultaneously.

Mechanical properties were measured using a variety of tests, both as a method of validating the material data provided by the manufacturer, and for observing the effects of different microstructures caused by different molding conditions on mechanical properties. Future work could include a micromechanics model linking the mechanical properties with the microstructure.

It was found that Flowcore had an inherent alignment even before molding, meaning that some aspect of the manufacturing process aligns the fibers slightly. It was also found that despite the relatively long length of these fibers (~50mm), experiencing significant flow or simple geometry changes in molding does not break the fibers. An interesting observation was that as the material is deformed within the mold further from its flat starting plane, the fiber orientation becomes more planarly oriented. This is believed to be because of the draping required to place the charge into the mold. Future work could

be done in fully exploring this phenomenon with parts that experience an even greater geometry change.

Future work on expanding the contribution of an expedited and more accurate microcomputed tomography technique could include the addition of a self-locating mechanism, for faster alignment of the scans in post-processing.

## References

- [1] T. W. Clyne, *An Introduction to Composite Materials Third Edition*. Cambridge University Press, 2019.
- [2] A. S. Björnsson, M. Jonsson, K. Johansen, “Automated material handling in composite manufacturing using pick-and-place systems – a review,” *Robotics and Computer-Integrated Manufacturing*, vol. 51, pp. 222-229, 2018.
- [3] W. Krause, F. Henning, S. Tröster, O. Geiger and P. Eyerer, “LFT-D – A Process Technology for Large Scale Production of Fiber Reinforced Thermoplastic Components,” *Journal of Thermoplastic Composite Materials*, Vol. 14, 2002.
- [4] R.C. Hibbeler, *Mechanics of Materials 10th Edition*, Pearson, 2017.
- [5] D. Krasteva, “Integrated Prediction of Processing and Thermomechanical Behavior of Long Fiber Thermoplastic Composites,” *Universidade do Minho*, 2009.
- [6] A. Bartos, J. Kocs, J. Anggono, J. Moczo, B. Pukanszky, “Effect of fiber attrition, particle characteristics and interfacial adhesion on the properties of PP/sugarcane bagasse fiber composites,” *Polymer Testing*, vol. 98, 2021.
- [7] M.D. Wakeman, T.A. Cain, C.D. Rudd, R. Brooks, A.C. Long, “Compression molding of glass and polypropylene composites for optimized macro- and micro-mechanical properties II. Glass-mat-reinforced thermoplastics,” *Composites Science and Technology*, vol.59, issue 5, pp. 709-726, 1999.
- [8] J. Dahl, p. Blanshard, T. Latimer, J. Sudria, J. Henshaw, “A Method for Characterizing Fiber Length Distribution in Random Fiber Composites,” *SPE Automotive*.
- [9] R.F. Gibson, *Principles of Composite Material Mechanics*, McGraw-Hill, 1994.
- [10] K. Ortman, D. Baird, P. Wapperom, A. Aning, “Prediction of Fiber Orientation in the Injection Molding of Long Fiber Suspensions,” *Polymer Composites*, 2012.
- [11] A. Motaghi, A. Hrymak, “Microstructure Characterization in Direct Sheet Molding Compound,” *Polymer Composites*, 2017.
- [12] F. Buck, B. Brylka, F. Henning, A. Hrymak, “Coupling of mold flow simulations with two-scale structural mechanical simulations: Modeling and experimental validation,” *Karlsruhe Institute of Technology*, 2014.
- [13] G.M. Vélez-Garcia, P. Wapperom, V. Kunc, D.G. Baird, A. Zink-Sharp, “Sample Preparation and image acquisition using optical-reflective microscopy in the measurement of fiber orientation in thermoplastic composites,” *Journal of Microscopy*, vol. 248, pt. 1, pp. 23-33, 2012.
- [14] L. Schottl, K.A. Weidenmann, T/ Sabiston, K. Inal, P. Elsner, “Fiber bundle tracking method to analyze sheet molding compound microstructure based on computed tomography images,” *NDT&E International*, vol. 117, 2021.

- [15] S.C. Garcea, Y. Wang, P.J. Withers, "X-ray computed tomography of polymer composites," *Composites Science and Technology*, vol. 156, pp. 305-319, 2018.
- [16] T. Sabiston, K. Inal, P. Lee-Sullivan, "Method to determine the required microstructure size to be represented by a second order fiber orientation tensor using X-ray micro computed tomography to evaluate compression molded composites," *Composites Science and Technology*, vol. 182, 2019.
- [17] C. Xu, A. Hrymak, F. Henning, "Material Properties and Heat Transfer Parameters in Compression Molding of Glass Mat Thermoplastics" (2020). Electronic Thesis and Dissertation Repository. 7436.
- [18] J.M. Hodgkinson, *Mechanical Testing of Advanced Fiber Composites*, Woodhead Publishing Limited, 2000.
- [19] W.S. Rasband, "ImageJ," U. S. National Institutes of Health, Bethesda, Maryland, USA, <https://imagej.nih.gov/ij/>, 1997-2018.
- [20] P. Pinter, S. Dietrich, B. Bertram, L. Kehrer, P. Elsner, K.A. Weidenmann, "Comparison and error estimation of 3D fiber orientation analysis of computed tomography image data for fiber reinforced composites," *NDT & E International*, vol. 95, pp. 26-35, 2018.
- [21] "MATLAB," version 7.10.0 (R2010a), The MathWorks Inc., 2010.
- [22] K. Harrington, M. Cieslinski, D. Baird, "MOE\_1, MOE\_2, MOE\_3," Virginia Tech University, 2013.
- [23] ASTM D638-14, "Standard Test Method for Tensile Properties of Plastics," vol. 08.01, DOI: 10.1520/D0638-14.
- [24] ASTM D7264/D7264M-21, "Standard Test Method for Flexural Properties of Polymer Matrix Composite Materials," vol. 15.03, DOI: 10.1520/D7264\_D7264M-21.
- [25] ASTM D3171-11, "Standard Test Methods for Constituent Content of Composite Materials," vol. 15.03, DOI: 10.1520/D3171-11.
- [26] LANXESS, "Flowcore Material Data Sheet", provided by Ryan Gergely, 2017.
- [27] T. Chang, A. Hrymak, F. Henning, "Characterization of Material for Composite Automotive Components," 2021.
- [28] W. G. Cochran, "The distribution of quadratic forms in a normal system, with applications to the analysis of covariance," *Mathematical Proceedings of the Cambridge Philosophical Society*, vol. 30 (2), pp. 178–191, 1934.
- [29] J.L. Thomason, M.A. Vlug, G. Schipper, H.G.L.T. Krikor, "Influence of fibre length and concentration on the properties of glass fibre-reinforced polypropylene: Part 3. Strength and strain at failure," *Composites Part A: Applied Science and Manufacturing*, vol. 27, issue 11, pp. 1075-1084, 1996.
- [30] J. T. Hofmann, G.M. Vélez-Garcia, D.G. Baird, A.R. Whittington, "Application and Evaluation of the Method of Ellipses for Measuring the Orientation of Long, Semi-Flexible Fibers," *Polymer Composites*, vol. 34, pp. 390-398, 2013.

## Appendices

### Appendix A - Comparison of Average Values of Primary Components of Orientation $a_{11}$ and $a_{22}$ of Hat Section Secondary Locations

	$a_{11}$	$a_{22}$
J	0.348	0.428
F	0.353	0.487
B	0.415	0.429
D	0.380	0.453
Q	0.324	0.476

### Appendix B - Orientation Sampling Locations and Molding Conditions of Plaques

Sample Code	Part Date [ddmmyy]	Batch Number	Part Number	Sample Location	Mold Temp [°C]	Oven Temp [°C]	Heating Time [min]	Charge Coverage [%]	# Sheets	Sheet Thickness [mm]	Pressure [bar]
B1	190315	1	5	A	150	300	12	100	1	2	300
B2	190315	1	5	B	150	300	12	100	1	2	300
<b>B3</b>	<b>190315</b>	<b>1</b>	<b>5</b>	<b>C</b>	<b>150</b>	<b>300</b>	<b>12</b>	<b>100</b>	<b>1</b>	<b>2</b>	<b>300</b>
B4	190315	1	5	E	150	300	12	100	1	2	300
<b>B5</b>	<b>190315</b>	<b>1</b>	<b>5</b>	<b>F</b>	<b>150</b>	<b>300</b>	<b>12</b>	<b>100</b>	<b>1</b>	<b>2</b>	<b>300</b>
B6	190315	1	6	A	150	300	12	100	1	2	300
B7	190315	1	6	B	150	300	12	100	1	2	300
B8	190315	1	6	C	150	300	12	100	1	2	300
B9	190315	1	6	D	150	300	12	100	1	2	300
B10	190315	1	6	F	150	300	12	100	1	2	300
B11	190315	1	9	A	150	300	12	100	1	2	300
<b>B12</b>	<b>190315</b>	<b>1</b>	<b>9</b>	<b>B</b>	<b>150</b>	<b>300</b>	<b>12</b>	<b>100</b>	<b>1</b>	<b>2</b>	<b>300</b>
B13	190315	1	9	C	150	300	12	100	1	2	300

B14	190315	1	9	E	150	300	12	100	1	2	300
B15	190315	1	9	F	150	300	12	100	1	2	300
C1	191115	4	9	A	150	300	12	90	1	3	300
C2	191115	4	9	B	150	300	12	90	1	3	300
C3	191115	4	9	C	150	300	12	90	1	3	300
C4	191115	4	9	D	150	300	12	90	1	3	300
C5	191115	4	8	A	150	300	12	90	1	3	300
C6	191115	4	8	B	150	300	12	90	1	3	300
C7	191115	4	8	C	150	300	12	90	1	3	300
C8	191115	4	8	D	150	300	12	90	1	3	300
C9	191115	4	8	E	150	300	12	90	1	3	300
C10	191115	4	8	F	150	300	12	90	1	3	300
C11	191115	4	8	G	150	300	12	90	1	3	300
C12	191115	4	9	A	150	300	12	90	1	3	300
C13	191115	4	9	B	150	300	12	90	1	3	300
C14	191115	4	9	C	150	300	12	90	1	3	300
C15	191115	4	9	D	150	300	12	90	1	3	300
C16	191115	4	9	E	150	300	12	90	1	3	300
C17	191115	4	9	F	150	300	12	90	1	3	300
C18	191115	4	9	G	150	300	12	90	1	3	300
D1	191115	5	4	A	150	300	12	62.4	2	3	300
D2	191115	5	4	B	150	300	12	62.4	2	3	300
D3	191115	5	4	C	150	300	12	62.4	2	3	300
<b>D4</b>	<b>191115</b>	<b>5</b>	<b>4</b>	<b>D</b>	<b>150</b>	<b>300</b>	<b>12</b>	<b>62.4</b>	<b>2</b>	<b>3</b>	<b>300</b>
D5	191115	5	4	E	150	300	12	62.4	2	3	300
D6	191115	5	4	F	150	300	12	62.4	2	3	300
D7	191115	5	4	G	150	300	12	62.4	2	3	300
D8	191115	5	5	A	150	300	12	62.4	2	3	300
D9	191115	5	5	B	150	300	12	62.4	2	3	300

D10	191115	5	5	C	150	300	12	62.4	2	3	300
<b>D11</b>	<b>191115</b>	<b>5</b>	<b>5</b>	<b>D</b>	<b>150</b>	<b>300</b>	<b>12</b>	<b>62.4</b>	<b>2</b>	<b>3</b>	<b>300</b>
D12	191115	5	5	E	150	300	12	62.4	2	3	300
D13	191115	5	5	F	150	300	12	62.4	2	3	300
D14	191115	5	5	G	150	300	12	62.4	2	3	300
D15	191115	5	6	A	150	300	12	62.4	2	3	300
D16	191115	5	6	B	150	300	12	62.4	2	3	300
D17	191115	5	6	C	150	300	12	62.4	2	3	300
D18	191115	5	6	D	150	300	12	62.4	2	3	300
D19	191115	5	6	H	150	300	12	62.4	2	3	300
D20	191115	5	6	i	150	300	12	62.4	2	3	300
D21	191115	5	6	J	150	300	12	62.4	2	3	300

## Appendix C - Orientation Sampling Locations and Molding Conditions of Hat Sections

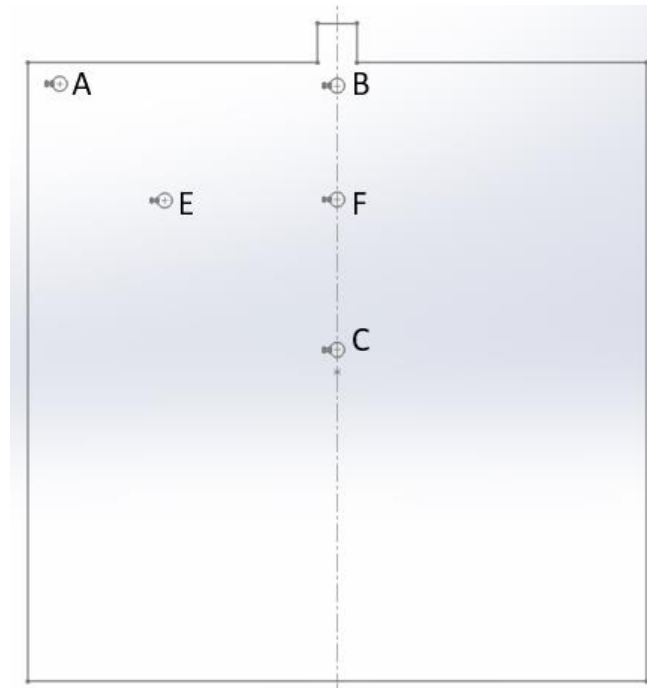
Sample Code	Part Date [ddmmyy]	Batch Number	Part Number	Sample Location	Mold Temp [°C]	Oven Temp [°C]	Heating Time [min]	Charge Coverage [%]	# Sheets	Sheet Thickness [mm]	Pressure [bar]
E1	200428	1	3	A	150	300	12	100	1	2	500
E2	200428	1	3	B	150	300	12	100	1	2	500
E3	200428	1	3	C	150	300	12	100	1	2	500
E4	200428	1	3	D	150	300	12	100	1	2	500
E5	200428	1	3	E	150	300	12	100	1	2	500
E6	200428	1	3	F	150	300	12	100	1	2	500
E7	200428	1	3	J	150	300	12	100	1	2	500
E8	200428	1	3	Q	150	300	12	100	1	2	500
E9	200428	1	4	A	150	300	12	100	1	2	500
E10	200428	1	4	B	150	300	12	100	1	2	500
E11	200428	1	4	C	150	300	12	100	1	2	500
E12	200428	1	4	D	150	300	12	100	1	2	500
E13	200428	1	4	E	150	300	12	100	1	2	500
E14	200428	1	4	F	150	300	12	100	1	2	500
E15	200428	1	4	J	150	300	12	100	1	2	500
E16	200428	1	4	Q	150	300	12	100	1	2	500
E17	200428	1	6	E	150	300	12	100	1	2	500
E18	200428	1	6	F	150	300	12	100	1	2	500
E19	200428	1	6	J	150	300	12	100	1	2	500
E20	200428	1	6	Q	150	300	12	100	1	2	500
E21	200428	1	7	J	150	300	12	100	1	2	500
E22	200428	1	7	Q	150	300	12	100	1	2	500
E23	200428	1	8	A	150	300	12	100	1	2	500
E24	200428	1	8	B	150	300	12	100	1	2	500
E25	200428	1	8	C	150	300	12	100	1	2	500



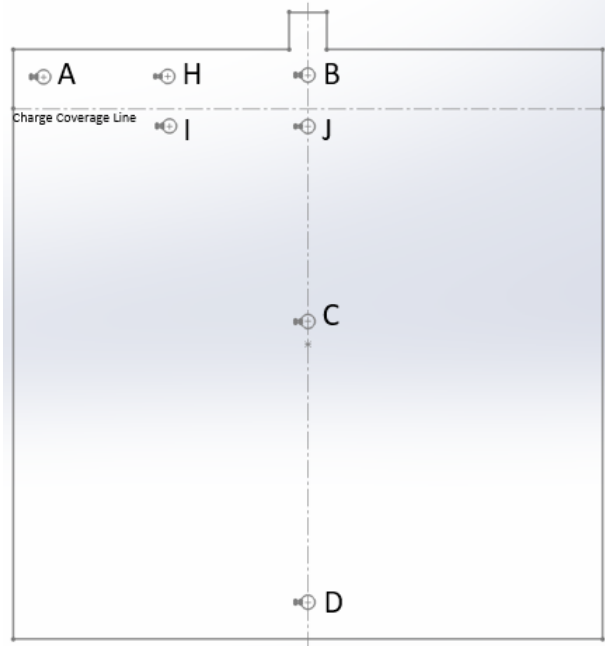
<b>E26</b>	<b>200428</b>	<b>1</b>	<b>8</b>	<b>D</b>	<b>150</b>	<b>300</b>	<b>12</b>	<b>100</b>	<b>1</b>	<b>2</b>	<b>500</b>
E27	200428	1	8	E	150	300	12	100	1	2	500
E28	200428	1	8	F	150	300	12	100	1	2	500
E29	200428	1	8	M	150	300	12	100	1	2	500
<b>E30</b>	<b>200428</b>	<b>1</b>	<b>8</b>	<b>N</b>	<b>150</b>	<b>300</b>	<b>12</b>	<b>100</b>	<b>1</b>	<b>2</b>	<b>500</b>
E31	200428	1	8	T	150	300	12	100	1	2	500
E32	200428	1	10	B	150	300	12	100	1	2	500
E33	200428	1	10	C	150	300	12	100	1	2	500
E34	200428	1	10	G	150	300	12	100	1	2	500
E35	200428	1	10	M	150	300	12	100	1	2	500
E36	200428	1	10	N	150	300	12	100	1	2	500
E37	200428	1	10	T	150	300	12	100	1	2	500
E38	200428	1	11	A	150	300	12	100	1	2	500
E39	200428	1	11	B	150	300	12	100	1	2	500
E40	200428	1	11	C	150	300	12	100	1	2	500
E41	200428	1	11	D	150	300	12	100	1	2	500
E42	200428	1	11	E	150	300	12	100	1	2	500
E43	200428	1	11	F	150	300	12	100	1	2	500
E44	200428	1	11	G	150	300	12	100	1	2	500
E45	200428	1	11	M	150	300	12	100	1	2	500
E46	200428	1	11	N	150	300	12	100	1	2	500
E47	200428	1	11	T	150	300	12	100	1	2	500
E48	200428	1	12	A	150	300	12	100	1	2	500
E49	200428	1	12	B	150	300	12	100	1	2	500
E50	200428	1	12	C	150	300	12	100	1	2	500
<b>E51</b>	<b>200428</b>	<b>1</b>	<b>12</b>	<b>D</b>	<b>150</b>	<b>300</b>	<b>12</b>	<b>100</b>	<b>1</b>	<b>2</b>	<b>500</b>
E52	200428	1	12	E	150	300	12	100	1	2	500
E53	200428	1	12	F	150	300	12	100	1	2	500
E54	200428	1	12	G	150	300	12	100	1	2	500

## Appendix D - Orientation Sampling Location Figures and Associated Sample Numbers

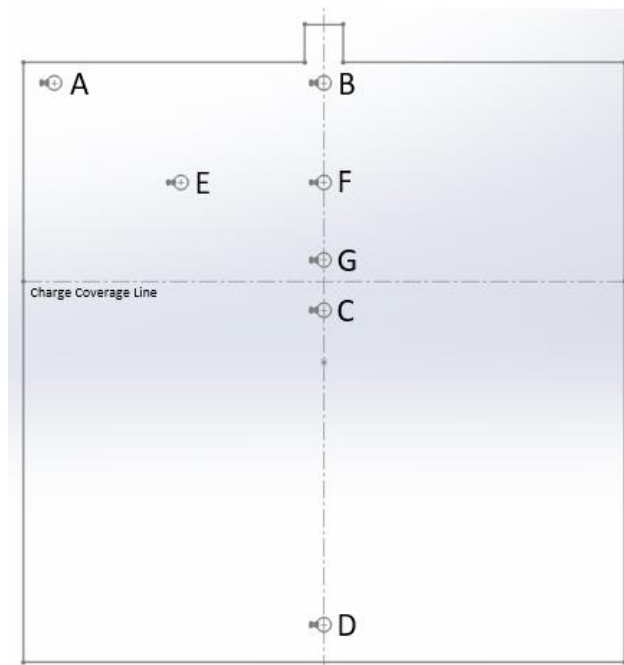
Plaque 100% Coverage, Samples B1-B15



## Plaque 90% Coverage, Samples C1-C18



## Plaque 62.4% Coverage, Samples D1-D21



## Hat Section, Samples E1-E54

G					J					M	
E					F						
A										3 Raised Sections	
										B	
C					D						
N					Q					T	

## Curriculum Vitae

**Name:** Broderic Clement-Thorne

**Post-secondary Education and Degrees:** University of Western Ontario  
London, Ontario, Canada  
2014-2018 B.E.Sc. Mechanical and Materials Engineering

The University of Western Ontario  
London, Ontario, Canada  
2019-2022 M.E.Sc. Mechanical and Materials Engineering

**Related Work Experience:** Teaching Assistant  
The University of Western Ontario  
2019-2020